

## Chapter 11

# PHYSICAL ADSORPTION CHARACTERIZATION OF ORDERED AND AMORPHOUS MESOPOROUS MATERIALS

MATTHIAS THOMMES

*Quantachrome Instruments, 1900 Corporate Drive, Boynton Beach FL-33426, USA*  
*E-mail: [matthias.thommes@quantachrome.com](mailto:matthias.thommes@quantachrome.com)*

Gas adsorption is a widely used method for the characterization of mesoporous materials with regard to the determination of surface area, pore size, pore size distribution, and porosity. Significant progress was achieved during recent years with regard to the understanding of sorption phenomena in narrow pores and the subsequent improvement in the pore size analysis of porous materials, mainly because of the following reasons: (i) the discovery of novel ordered mesoporous materials, such as MCM-41, MCM-48, SBA-15, which exhibit a uniform pore structure and morphology and can therefore be used as model adsorbents to test theories of gas adsorption; (ii) carefully performed adsorption experiments (iii) the development of microscopic methods, such as the Non-Local Density Functional Theory (NLDFT) or computer simulation methods (e.g. Monte-Carlo – and Molecular-Dynamic simulations), which allow to describe the configuration of adsorbed molecules in pores on a molecular level. However, the influence of pore geometry, geometrical and chemical disorder (as present in many adsorbents) on adsorption, pore condensation and sorption hysteresis, and thus the shape of the sorption isotherm, remains under investigation.

## 1 Introduction

Porous materials are of great practical interest for applications in the chemical, oil and gas, food and pharmaceutical industries. Microporous materials (pore width < 2 nm [1]) such as zeolites are widely used in industry as heterogeneous catalysts, in oil refining and petrochemistry, however their applications are limited because of the narrow sizes of their cavities and channels. Mesoporous materials (pore widths: 2-50 nm [1]) as for instance silica gels, porous glasses, aerogel, mesoporous titania and alumina and others are widely used in applications related to separation science, catalysis etc. The successful performance of these applications requires a comprehensive characterization of these porous materials with regard to pore size, surface area, porosity and pore size distribution. Common mesoporous materials such as silica gels and porous glasses are amorphous; in contrast materials like zeolites are crystalline, i.e., every atom can be located in a microscopically-sized unit cell. Such symmetry is not present in amorphous materials. Whereas a complete and comprehensive characterization can be performed in case of crystalline

materials, amorphous nanoporous materials vary considerably in their microstructure and a complete and comprehensive characterization is problematic. However, average properties such as porosity, specific surface area, mean pore size and pore size distribution can still be determined.

Within this context, the in 1992 by Mobil scientists [2] discovered silicate/ aluminosilicate mesoporous molecular sieves of the M41S family (i.e, MCM-41, MCM-48, MCM-50) are very interesting [e.g, 2-4]. These materials are synthesized by using surfactants as structure directing agents and can be characterized by well defined pores of tunable sizes in the range between 2 nm and 10 nm, and specific surface areas between 600 m<sup>2</sup>/g and 1300 m<sup>2</sup>/g. The most prominent representatives of M41S materials are MCM-41 and MCM-48. MCM-41 consists of regular pseudo-one-dimensional pores in a honeycomb arrangement while MCM-48 exhibits cubic symmetry consisting of two interwoven, but unconnected three-dimensional pore systems of cylindrical pores. MCM-50 comprises a lamellar phase. Independently, a family of mesoporous silica materials of similar properties as MCM-41 was discovered by Japanese researchers [5,6]; a prominent member of this family is for instance FSM-16 [6]. These mesoporous molecular sieves are essentially amorphous on a microscopic scale (i.e., the pore walls) but can be considered as highly ordered on larger (macroscopic) length scales, and exhibit therefore properties of both zeolites and mesoporous solids such as silica gels and porous glasses. While the pore diameter range of MCM-41 materials is restricted to ca. 10 nm, ordered mesoporous silica molecular sieves with pore diameter up to ca. 30 nm (SBA-15) can be obtained by using amphiphilic block copolymers as templates [e.g,7]. SBA-15 similar to MCM-41 consists of a hexagonal packing of cylindrical channels – but depending on details of the synthesis procedure this material can possess irregular intrawall micro-mesopores, which connect adjacent channels [8,9]. MCM-48 material is more difficult to synthesize and typically high-quality materials can be obtained in the pore size range between 2 and ca. 5 nm [12]. Meanwhile a great variety of mesoporous molecular sieve materials has been synthesized among them also materials with well defined cage-like structures (e.g., SBA-2, SBA-12, SBA-16). Mesoporous molecular sieves have potential applications in catalysis, separations [10], guest-host technologies etc [11,12]. Other recently developed ordered mesoporous materials include periodic mesoporous organosilicas (PMO's) [e.g., 13,14,15], nanoporous carbons with ordered mesostructure (e.g, CMK1, CMK3 ) [e.g.,16, 17] porous metal-organic framework materials [18 ] and carbon nanotubes [e.g.,19].

The high degree of order in M41S materials compared to conventional mesoporous materials is reflected in a narrow pore size distribution, which is determined by assuming that the porous material consists of pores having the same (cylindrical) shape, but varying only in size. This is illustrated in figure 1, which shows the extremely sharp pore size distribution curves (PSD) of MCM-41, and SBA-15 compared to the much broader PSD's for controlled-pore glass samples (CPG). The pore size distributions shown in figure 1 were obtained from nitrogen adsorption isotherms (at 77 K) [20]. Gas adsorption is one of many experimental methods available for the characterization of porous materials. These include small angle x-ray and neutron scattering (SAXS and SANS), mercury porosimetry, electron microscopy (scanning and transmission), thermoporometry, NMR-methods, and others. Each method has a limited length scale of applicability for pore size analysis. An overview of different methods for pore size characterization and their application range was recently given by IUPAC [21]. Among these methods gas adsorption is the most popular one because it allows to assess a wide range of pore sizes (from 0.35 nm up to 100 nm) including the complete range of micro- and mesopores and even macropores. In addition, gas adsorption techniques are convenient to use and are not that cost intensive as compared to some of the other methods.

The adsorbed amount as a function of pressure can be obtained by volumetric (manometric) and gravimetric methods, carrier gas and calorimetric techniques, nuclear resonance as well as by a combination of calorimetric and impedance spectroscopic measurements [22 - 24]. Surface area and pore size analysis is usually based on nitrogen, argon and krypton adsorption isotherms obtained with the volumetric (manometric) method at temperatures of liquid nitrogen (77.35 K) and liquid argon (87.27 K). The shape of adsorption/desorption isotherms (i.e., sorption isotherm) depends on pore size and temperature, i.e., differences in the thermodynamic states of the pore fluid and the bulk fluid (which includes critical point and triple point shifts of the pore fluid as compared to the bulk fluid; see section 3.2) as well as on the chemical and geometrical heterogeneity (i.e. the degree of disorder) of the porous material. For instance, the pore size characterization of mesoporous materials is based on an accurate understanding of the pore condensation phenomenon, which is characterized by a step in the sorption isotherm. Pore condensation represents a confinement induced shifted gas-liquid phase transition, i.e., condensation occurs at a pressure  $P$  less than the saturation pressure  $P_0$  of the fluid. The  $P/P_0$ -value where pore condensation occurs depends on the

liquid-interfacial tension, the strength of the attractive interactions between the fluid and pore walls, the pore geometry and the pore size.

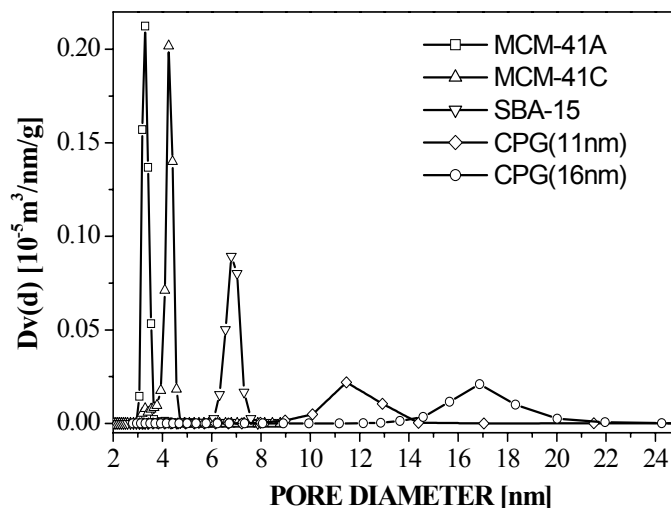


**Figure 1.** Pore size distribution curves for mesoporous molecular sieves (MCM-41 SBA-15), and controlled-pore glasses obtained from  $N_2$  (77K) sorption isotherms. From [20].

A relation between the pore size and the pore condensation/evaporation pressure for a given fluid/pore system is for instance given by the classical Kelvin equation. Pore condensation is often accompanied by hysteresis, i.e., evaporation of the condensed fluid (desorption branch of the hysteresis loop) occurs at a lower pressure as compared to pore condensation, which complicates the situation. The decision whether the adsorption – or desorption branch of the sorption isotherm should be taken for the pore size analysis is often crucial for an accurate pore size analysis.

Despite the sometimes very complex microstructure of adsorbents the theoretical models and methods, which are applied to analyse sorption isotherms are commonly based on extremely simplified assumptions of the texture of the porous material. In almost all cases it is assumed that the adsorbent consists of an assembly of independent pores of given geometry (e.g., cylindrical or slit-like) with the additional assumption that the pore walls are chemically and geometrically homogeneous. Hence, the total adsorption isotherm consists of a sum of adsorption isotherms over a distribution of narrow pores. In order to test theoretical models which describe the relationship between the shape of an isotherm, pore size and texture, model adsorbents are needed, which reflect the assumptions made in the theoretical models. Mesoporous molecular sieves and in particular MCM-41 were already early recognized as good candidates for the testing

of theoretical models of gas adsorption, mainly because of two reasons: (i) the periodicity of mesoporous molecular sieves allows to use other techniques such as high resolution transmission electronic microscopy (TEM) and methods based on X-ray diffraction (XRD) to compare with pore size results obtained from gas adsorption; (ii) MCM-41 consists of independent pseudo-one-dimensional pores of well defined (hexagonal /cylindrical) pore geometry. Despite the fact that the pore channels may exhibit some curvature [25], MCM-41 silica material still captures the most important features of theoretical models currently used for pore size analysis.

Within this framework extensive experimental and theoretical studies on the sorption and phase behavior of fluids in ordered mesoporous molecular sieves have been performed since the first systematic sorption studies on MCM-41 had been published in 1993 [26,27]. Most of the following work focussed again on the adsorption properties of MCM-41 materials [e.g., 26-37], but somewhat later (starting at ca. 1996), systematic adsorption studies were also performed on other mesoporous silica molecular sieves such as SBA-15 [e.g. 9,38-40], MCM-48 [41-48], FSM-16 etc.. [e.g., 49,50]. The systematic evaluation of the adsorption properties of PMO and CMK adsorbents [e.g. 51] is in progress.

In particular, the studies involving MCM-41 materials have revealed, that classical methods for mesopore size analysis based on macroscopic, thermodynamic assumptions (e.g., methods based on the Kelvin equation) cannot describe the sorption and phase behavior of fluids in narrow mesopores correctly, which leads to an underestimation of the pore size up to ca. 25 % for materials consisting of pores < ca. 10 nm. Subsequently performed corrections of the Kelvin equation based methods have indeed led to some improvement in the accuracy, but only over a limited pore size range. An accurate mesopore size analysis over the complete micro- and mesopore size range is possible by applying microscopic methods based on statistical mechanics, such as the Non-Local Density Functional Theory (NLDFT) or computer simulation methods (Grand Canonical Monte Carlo (GCMC) and Molecular-Dynamic (MD) simulations). These methods allow to describe the configuration of adsorbed molecules in pores on a molecular level. Pore size analysis data for mesoporous molecular sieves obtained with these methods agree very well with the results obtained from independent methods (based on XRD, TEM etc.). In contrast to the classical methods, the microscopic methods for pore size analysis take into account details of the fluid-fluid interactions and the adsorption potential (which depends on the strength of the fluid-wall interactions and the pore geometry). Appropriate methods for pore size analysis based on

NLDFT and GCMC are meanwhile commercially available for many important fluid/substrate systems.

Despite this progress, a satisfying verification of theoretical models for mesopore size analysis is only achieved so far for highly ordered materials (e.g. mesoporous molecular sieves), which can be modeled within the framework of an independent pore model. Theories based on a single pore models may be in some cases (to some extend) applicable to describe the sorption and phase behavior of fluids in disordered materials, but this is not generally the case. The mechanisms of adsorption, pore condensation and hysteresis in disordered mesoporous materials is still not completely understood and more theoretical and experimental work is clearly required to understand the combined effects of confinement, pore geometry, connectivity etc., on the origin of pore condensation and hysteresis. The application of models which attempt to describe the microstructure of porous materials at length scales beyond that of a single pore is under investigation.

The paper is organized as follows: In section 2 we discuss some general aspects of the application of physical adsorption for surface and pore size analysis. Recent advances in the understanding of sorption, pore condensation, hysteresis phenomena, and critical behavior of fluids confined to mesoscopic systems will be reviewed in section 3. Important consequences for pore size calculation will be discussed in section 4. A discussion of the accuracy and applicability of classical, thermodynamic methods for pore size analysis compared to microscopic models (e.g. NLDFT) can also be found in section 4. Concluding remarks will be given in section 5.

## 2 Surface and pore size analysis by physisorption: General aspects

### 2.1 Physisorption measurement

Physical adsorption of gases on solid surfaces is caused by the attractive van der Waals interactions (i.e., dispersion forces) of gas molecules (adsorptive) with a solid (adsorbent). The interaction energy  $U_s(z)$  of a gas molecule at distance  $z$  from a solid surface is approximately given as:

$$U_s(z) = -(\pi/6)C_{sf}\rho_s/z^3 \quad (1)$$

where  $C_{sf}$  is a measure for the strength of attractive fluid-wall interactions and  $\rho_s$  represents the solid density. At sufficiently low temperatures (typically at and below the normal boiling temperature of the adsorptive),

the adsorption of gases can be analyzed in terms of a two-phase model in which an adsorbed phase (adsorbate) coexists with the bulk phase. This is the typical situation encountered for nitrogen, argon and krypton adsorption at the temperatures of liquid nitrogen (ca. 77.35 K) and liquid argon (ca. 87.27 K), respectively. The amount of adsorbed fluid can be expressed by the adsorbed mass of gas or volume (often given in STP per unit mass; STP: standard temperature and pressure, namely 273.15 K, 760 Torr, i.e.  $1.01325 \times 10^5$  Pa).

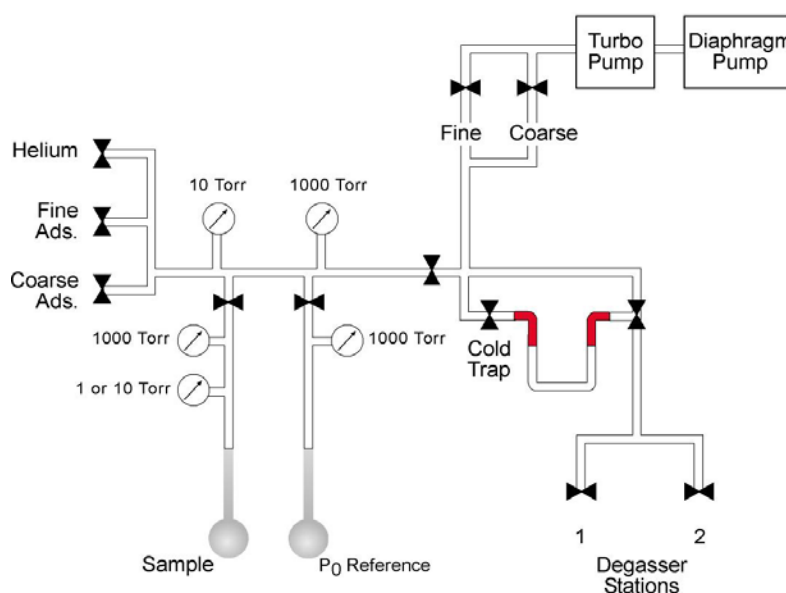


**Figure 2.** Schematic illustration of a volumetric (manometric) adsorption apparatus.

The volumetric (manometric) method is generally applied for adsorption measurements at cryogenic temperatures. The method is based on the measurement of the gas pressure in a calibrated constant volume, at known temperature. An example for a state-of-the-art volumetric adsorption apparatus is given in the schematic figure 2. The analysis station of the volumetric sorption apparatus is equipped - in addition to the obligatory pressure transducers in the dosing volume (manifold) of the apparatus - with high precision pressure transducers dedicated to read the pressure just in the sample cell. Hence, the sample cell is isolated during equilibration, which ensures a very small effective void volume and therefore a highly accurate determination of the adsorbed amount. The saturation pressure  $P_0$

is measured throughout the entire analysis by means of a dedicated saturation pressure transducer, which allows the vapor pressure to be monitored for each data point. This leads to high accuracy and precision in the determination of  $P/P_0$  and thus in the determination of the pore size distribution. It is of advantage to use a diaphragm pump as a foreline pump for the turbomolecular pump in order to guarantee a complete oil-free environment for (i) the adsorption measurement and (ii) the outgassing of the sample, prior to the analysis.

## 2.2 Characterization of mesoporous materials

The International Union of Pure and Applied Chemistry (IUPAC) [1] proposed to classify pores by their internal pore width (the pore width defined as the diameter in case of a cylindrical pore and as the distance between opposite walls in case of a slit pore). *Micropore*: pore of internal width less than 2 nm; *mesopore*: pore of internal width between 2 and 50 nm; *macropore*: pore of internal width greater than 50 nm. In the same paper the IUPAC classification of sorption isotherms was published. The different shapes of the 6 isotherms in the classification reveal the influence of the interplay between the strength of attractive fluid-wall and fluid-fluid interactions as well as the effects of confined pore space on the shape of adsorption isotherms.

An analysis of gas adsorption isotherms allows to determine surface area, pore size, pore size distribution, pore volume, and porosity. In addition some information about the roughness of the adsorbent surfaces and fractal dimension can be obtained. The *specific surface area* is usually determined by the method of Brunauer Emmett and Teller (BET). By applying the BET equation in a relative pressure range between 0.05 – 0.3, the monolayer capacity  $N_m$  is determined. The specific surface area  $S$  is obtained from the monolayer capacity by the application of the simple equation:  $S = N_m L \sigma$ , where  $L$  is the Avogadro constant and  $\sigma$  is the so-called cross-sectional area (the average area occupied by each molecule in a completed monolayer). The BET equation is applicable for surface area analysis of nonporous- and mesoporous materials consisting of pores of wide pore diameter, but is in a strict sense not applicable in case of microporous adsorbents (a critical appraisal of the BET method is given in refs. [52-54]). In addition it seems that the BET method is inaccurate for estimating the surface area of mesoporous molecular sieves of pore widths  $< ca. 4$  nm, because pore filling is observed at pressures very close to the pressure range where monolayer-multilayer formation on the pore walls occurs, which may lead to a significant overestimation of the monolayer



capacity in case of an BET analysis. In addition, the result depends very much on the assumed cross-sectional area. For instance, recent experimental sorption studies on MCM-41 silica materials suggest strongly, that the cross-sectional area of nitrogen on a hydroxylated surface (as it is the case for MCM-41) might differ from the commonly adopted value of  $0.162 \text{ nm}^2$  [55]. Similar observation were already made in the past and it was assumed, that the quadrupole moment of the nitrogen molecule leads to specific interactions with the hydroxyl groups on the surface causing an orientating effect on the adsorbed nitrogen molecule [56]. A cross-sectional area of  $0.135 \text{ nm}^2$  was proposed, which was obtained by measuring the volume of  $\text{N}_2$  adsorbed on silica spheres of known diameter [57].

Because of the roughness of amorphous surfaces the determination of the *fractal dimension* by gas adsorption can be considered as a useful and characteristic parameter, which complements the surface and pore size characterization [58 - 60]. The determination of the surface roughness in the scale range of molecular sizes (usually less than  $10 \text{ \AA}$ ) can be obtained by means of the method of molecular tiling which is based on a comparison of the monolayer capacities of different adsorbents. The scale range from  $10\text{-}20 \text{ \AA}$  to  $1000 \text{ \AA}$  can be investigated by analyzing the multilayer region of a sorption isotherm by means of the Frenkel-Halsey Hill method. A thermodynamic method (the so-called Neimark-Kiselev (NK) method) allows to sense fractal properties of mesoporous materials in the range of scales from ca.  $4 \text{ \AA} - 1000 \text{ \AA}$ . For instance, a characterization of MCM-41 with regard to roughness and fractality over a wide range of length scales can be found in ref. [60]. Please note that the interpretation of fractal dimension parameters obtained by gas adsorption in the context of fractal self-similarity (and/or self-affinity) is not always justified.

In case that the sorption isotherm exhibits a distinct plateau (see isotherms in figure 2a, i.e., so-called IUPAC type IV and type V sorption isotherms), the *total specific pore volume* can be obtained by converting the amount adsorbed after the pore filling step into liquid volume assuming that the density of the adsorbate is equal to the bulk liquid density at saturation (so-called Gurvich rule). The gas adsorption technique allows of course only to determine the volume of open pores. Closed porosity cannot be accessed, but can be derived if the true density and particle(bulk) density of the materials are known. *Porosity* is defined as the ratio of the volume of pores and voids to the volume occupied by the solid. If a cylindrical pore geometry can be assumed, the *average pore diameter* of a porous materials can be calculated by the following relation:

$$D_{4V/s} = 4V_p/(S_{total} - S_{ext}) \quad (2)$$

The total surface area  $S_{total}$  can be calculated either from the BET-method, from t-plot or  $\alpha_s$  comparison plot methods [52]. The external surface area can be determined by applying for instance the comparison plot method in the region of relative pressure above the pore condensation step.

In order to obtain a comprehensive surface and pore size analysis from sorption isotherms, details about the pore condensation and hysteresis mechanism need to be known. This will be discussed in section 3.

### 2.3 Adsorptives other than nitrogen for mesopore analysis

Generally, nitrogen adsorption at liquid nitrogen temperature (77 K) is used for surface and pore size characterization. Krypton adsorption at 77 K is more or less exclusively used for low surface area analysis [52-54]. Argon adsorption at 77 K and liquid argon temperature (87 K) is also often used for micro- and mesopore size analysis. The use of argon adsorption is of advantage for the pore size analysis of zeolites and other microporous materials because the filling of pores of dimension 0.5 - 1 nm occurs at much higher relative pressure as compared to nitrogen adsorption. This phenomenon is related to the fact, that the nitrogen molecule possesses a quadrupole moment, which leads to specific fluid-wall interactions [54]. However, a combined and complete micro- and mesopore size analysis with argon is not possible at liquid nitrogen temperature (which is ca. 6.5 K below the triple point temperature of bulk argon). Systematic sorption experiments indicate that the pore size analysis of mesoporous silica by argon adsorption at 77 K is limited to pore diameters smaller than ca. 15 nm, i.e., pore condensation cannot be observed anymore above this pore size limit [20, 44]. This behavior is related to confinement effects on the location of the (quasi)-triple point of the pore fluid (see section 3.2). Of course, such a limitation does not exist for argon sorption at 87.27 K; pore filling and pore condensation can be observed here over the complete micro- and mesopore size range. Argon sorption isotherms obtained at 87 K and 77 K in ordered and disordered mesoporous silica materials of various mean pore size are shown in Figures 3a and b (the pore size distribution curves of these materials are given in Figure 1.) The argon sorption data at 87 K (in MCM-41, SBA-15 and controlled pore glasses) shown in Figure 3a reveal that pore condensation shifts to higher relative pressures with increasing pore diameter. In addition, hysteresis occurs in

all materials, with the exception of MCM-41 A (pore size: 3.3 nm), which exhibits reversible pore condensation. With increasing pore diameter, hysteresis begins to develop and is present for MCM-41 C (4.2 nm), and a wide hysteresis loop is observed for SBA-15 (6.7 nm).

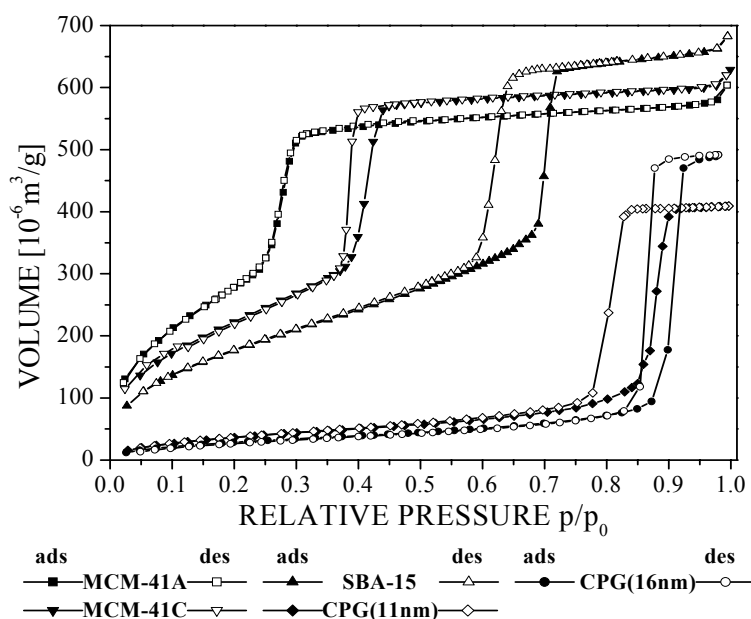


**Figure 3a.** Argon sorption isotherms at 87 K on MCM-41, SBA-15 and controlled-pore glasses (CPG) From [20].

The data also clearly reveal, that the width of the hysteresis loop increases with increasing pore size (details of the pore condensation and hysteresis mechanism will be discussed in section 3). Lowering the measurement temperature to 77 K (Figure 3b) leads to a widening of the hysteresis loops for the MCM-41 and SBA-15 silica samples (hysteresis appears also for MCM-41 A), but pore condensation and hysteresis cannot be observed anymore in the controlled pore glass of mode pore diameter 16 nm (the small deviations between the two argon sorption isotherms for CPG (16 nm) at 77 K are attributed to small differences in the temperature of the liquid nitrogen bath). A detailed analysis of the data in combination with the pore size distribution curves has led to the conclusion that pore condensation does not occur anymore for pore sizes larger than ca. 15 nm [20], which limits (as indicated before) the pore diameter range over which mesopore size analysis can be performed using argon as adsorptive at 77 K.

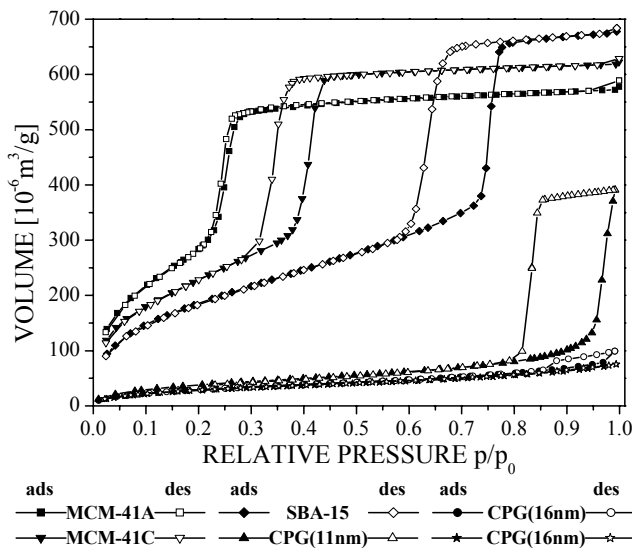


**Figure 3b.** Argon sorption at 77 K on MCM-41, SBA-15 and CPG. ( $P_0$  refers to solid argon). From [20].

### 3 Pore condensation and adsorption hysteresis

#### 3.1 The modified Kelvin equation

For pores of uniform shape and width (ideal slit-like or cylindrical mesopores) pore condensation can be described on the basis of the Kelvin equation, i.e., the shift of the gas-liquid phase transition of a confined fluid from bulk coexistence, is expressed in macroscopic quantities like the surface tension  $\gamma$  of the bulk fluid, the densities of the coexistent liquid  $\rho^l$  and gas  $\rho^g$  ( $\Delta\rho = \rho^l - \rho^g$ ) and the contact angle  $\theta$  of the liquid meniscus against the pore wall. For cylindrical pores the modified Kelvin equation [52-54] is given by

$$\ln(P/P_0) = -2\gamma\cos\theta / RT\Delta\rho(r_p - t_c), \quad (3)$$

where  $R$  is the universal gas constant,  $r_p$  the pore radius and  $t_c$  the thickness of an adsorbed multilayer film, which is formed prior to pore condensation. The occurrence of pore condensation is expected as long as the contact angle is below  $90^\circ$ . A contact angle of  $0^\circ$  is usually assumed in case of nitrogen and argon adsorption at 77 K and 87 K, respectively.

The Kelvin equation provides a relationship between the pore diameter and the pore condensation pressure, and predicts that pore condensation shifts to a higher relative pressure with increasing pore diameter and temperature. The modified Kelvin equation (eq. 3) serves as the basis for many methods applied for mesopore analysis, including the Barrett-Joyner Halenda method (BJH) [61], which is widely used. In order to account for the preadsorbed multilayer film, the Kelvin equation is combined with a standard isotherm or a so-called t-curve, which usually refers to adsorption measurements on a non-porous solid. Accordingly, the preadsorbed multilayer film is assessed by the statistical (mean) thickness of an adsorbed film on a nonporous solid of a surface similar to that of the sample under consideration (such statistical thickness equations were derived for instance by Halsey, Harkins-Jura and de-Boer [52-54]). However, it is obvious that assuming the situation of a nonporous, planar surface for the evaluation of the preadsorbed film thickness cannot be valid anymore in case of narrow pores, where the curvature of the pore walls and their adsorption potential has a pronounced effect on the film thickness and its interfacial tension. The corresponding inaccuracy in the pore size analysis is discussed in section 4.

### *3.2. Sorption and phase behavior of fluids in mesopores: multilayer adsorption, pore condensation and critical behavior*

In case of complete wetting, the pore walls are covered by a multilayer adsorbed film at the onset of pore condensation. The stability of this film is determined by the attractive fluid-wall interactions, the surface tension and curvature of the liquid-vapor interface. Multilayer adsorption can for instance be described in the spirit of the Frenkel-Halsey-Hill theory [52,54]. One of the basic assumptions is that the (sufficiently thick) adsorbed multilayer film can be considered as a slab of liquid, which reveals the same properties (i.e., density etc.) as the bulk liquid would have at this temperature. The only modification to its free energy arises from the interaction with the solid, i.e, the adsorption forces (dispersion forces). The chemical potential difference  $\Delta\mu = \mu - \mu_0$  of an adsorbed, liquid-like film of thickness  $t$  compared to the chemical potential of the appropriate bulk liquid ( $\mu_0$ ) is given according to the Frenkel-Halsey-Hill (F.H.H) equation by

$$\Delta\mu = \mu - \mu_0 = -\alpha t^{-m} \quad (4)$$

where  $\alpha$  is the fluid-wall interaction parameter, and the  $t^{-m}$  law results from the long-range van der Waals interactions between a fluid molecule and a semi-infinite planar wall. In case of non-retarded van der Waals fluid-wall interactions the exponent  $m$  has a theoretical value of 3. However, experimental values for  $m$  are often significantly smaller than the theoretical value, even for strongly attractive adsorbents like graphite, i.e.,  $m = 2.5 - 2.7$ . Among other reasons these deviations from the theoretical value are correlated with the surface roughness and the fractal nature of the pore wall [58,59].

The film thickness cannot grow unlimited in pores. The stability of the multilayer adsorbed film is determined by the long-range van der Waals interactions, and by the surface tension and curvature of the liquid-vapor interface. The chemical potential difference  $\Delta\mu$  is then given by

$$\Delta\mu = \Delta\mu_a + \Delta\mu_c \quad (5)$$

For small film thickness the first term  $\Delta\mu_a$  associated with multilayer adsorption dominates. When the adsorbed film becomes thicker, the adsorption potential will become less important, and  $\Delta\mu$  will be dominated almost entirely by the curvature contribution  $\Delta\mu_c$  (i.e., the Laplace term), which is given for cylindrical pores by  $\Delta\mu_c = -(\gamma/a) \Delta\rho$ ,  $a$  is the core radius ( $a = r_p - t$ ). At a certain critical thickness  $t_c$  pore condensation occurs in the core of the pore, controlled by intermolecular forces in the core fluid.

Figure 4 shows a (schematic) sorption isotherm as it is expected for adsorption/desorption of a pure fluid in a single mesopore of cylindrical shape in combination with a schematic representation of the appropriate sorption and phase phenomena occurring in the pore. Please note, that the schematic isotherm reveals a vertical pore condensation step. However, a truly vertical step in the adsorption isotherm is not to be expected for any real porous material with a nonvanishing pore-size distribution, i.e., the wider the pore size distribution, the less sharp is the observed pore condensation transition. The adsorption mechanism in mesopores is at lower relative pressures absolutely similar as in case of adsorption on planar surfaces. After completion of the monolayer formation (**A**), multilayer adsorption commences (**B**). After reaching a critical film thickness (**C**) capillary condensation occurs essentially in the core of the pore (transition from configuration **C** to **D**). The plateau region of the isotherm reflects the situation of a pore completely filled with liquid. The pore liquid is separated from the bulk gas phase by a hemispherical

meniscus. Pore evaporation therefore occurs by a receding meniscus (E) at a pressure, which is less than the pore condensation pressure.

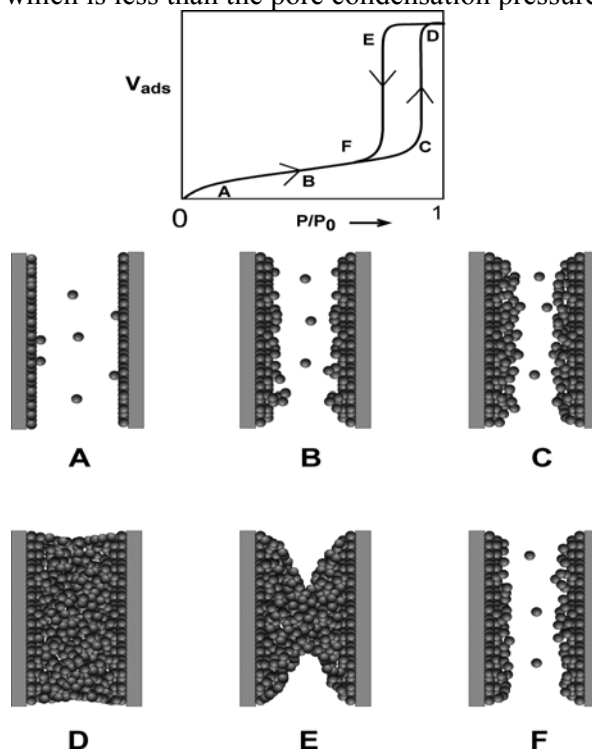


**Figure 4.** Schematic representation of multilayer adsorption, pore condensation and hysteresis in a single pore.

The pressure where the hysteresis loop closes corresponds again to the situation of an adsorbed multilayer film which is in equilibrium with a vapor in the core of the pore and the bulk gas phase. In the relative pressure range between (F) and (A) adsorption and desorption are reversible.

In contrast to the Kelvin approach, the Broeckhoff and de Boer [62 - 64] as well as the Saam-Cole theory [65] capture essentially the mechanism of pore condensation and hysteresis as it is described in Figure 4. These theories take into account the (i) influence of the adsorption potential on the chemical potential where pore condensation occurs in the pores and (ii) the effect of curvature on the thickness of the adsorbed multilayer film. In agreement with experimental observations, these theories predict that an increase in the strength of the attractive fluid-wall interaction, a lowering of the experimental temperature as well as

decreasing the pore size will shift the pore condensation transition to lower relative pressures.

However, all these thermodynamic, macroscopic theories do not account for the peculiarities of the critical region. As discussed before, the Kelvin approach considers pore condensation as a gas-liquid phase transition in the core of the pore between two homogenous, bulk like gas and liquid phases. The density difference  $\Delta\rho = \rho^l - \rho^g$  is considered to be equal to the difference in orthobaric densities of coexisting bulk phases, i.e., pore condensation and hysteresis are expected to occur up to the bulk critical point, where  $\Delta\rho = 0$ .

In contrast, microscopic approaches such as DFT [66], lattice model calculation [67] and various computer simulation studies [68-70] suggest that a fluid confined to a single pore can exist with two possible density profiles corresponding to inhomogeneous gas- and liquid configurations in the pore. In this sense pore condensation reflects a first order phase transition between an inhomogeneous gas configuration, which consists of vapor in the core region of the pore in equilibrium with a liquid like adsorbed film (corresponds to configuration **C** in figure 4), and a liquid configuration, where the pore is filled with liquid (corresponds to configuration **D** in figure 4). At the pore critical point of the confined fluid, these two hitherto distinct fluid configurations will become indistinguishable, i.e., a pore condensation step cannot be observed anymore. The suggested order parameter for this phase transition is here the difference in surface excess (or adsorbed amounts at low bulk gas densities, i.e.,  $\Delta V_{(l,g)} = V_{\text{ads(liquid)}} - V_{\text{ads(gas)}}$ ) between the two inhomogeneous gas and liquid phases and not the difference in orthobaric densities  $\Delta\rho$  as it is the case for the correspondent bulk phase transition, which occurs between homogeneous gas and liquid phases. Accordingly, at the pore critical point  $\Delta V_{(l,g)} = 0$  and pore condensation cannot be observed anymore. The critical temperature of the confined fluid is shifted to lower temperatures, i.e., in contrast to the predictions of the Kelvin equation pore condensation and hysteresis will vanish already at temperatures below  $T_c$ . The shift of the critical temperature can be rationalized by the argument that a fluid in narrow pores is an intermediate between a three-dimensional fluid and a one-dimensional fluid for which no critical point exists at  $T > 0$ . Hence, the shift of the pore critical temperature is correlated with the pore width, i.e., the more narrow the pore, the lower the pore critical temperature. Consequently, at a given subcritical temperature pore condensation is only possible in pores which are wider than the critical pore size  $W_c$ .



Adsorption experiments of pure fluids in porous glasses [71-73], silica gel [74] and MCM-41-type of materials [28b,75-77] revealed that pore condensation and hysteresis indeed disappears below the bulk critical temperature. Furthermore, systematic adsorption studies of SF<sub>6</sub> in controlled-pore glasses indicated already, that hysteresis already disappears below the pore critical temperature  $T_{cc}$ , i.e., reversible pore condensation could be observed (the criterion applied here to determine pore criticality was the disappearance of the pore condensation step) [73]. An experimental study on nitrogen adsorption in MCM-41 silica in combination with the application of density functional theory clearly revealed that the experimental disappearance of hysteresis is indeed not identical with having achieved the pore critical point [33]. Nitrogen sorption hysteresis (at 77 K) disappears when the pore diameter is smaller than 4 nm, however based on the theoretical results the (pseudo)-pore critical point is achieved at a much smaller pore diameter, i.e. 1.8 nm (the bulk critical temperature of nitrogen is 126.2 K). This picture was supported by subsequent experimental sorption studies of pure fluids in ordered mesoporous silica materials [75-77]. For instance, experiments to study the temperature dependence of argon adsorption in a MCM-41 materials with pore channels of 2.2 nm diameter revealed a hysteresis critical temperature  $T_h$  of ca. 62 K, whereas the pore critical temperature was located at ca. 98 K (the bulk critical temperature  $T_c$  for argon is 150.7 K), i.e., substantial downward shifts in the pore critical- and hysteresis critical temperatures are observed for such narrow pores [76,77]. These systematic studies also revealed that temperature and pore size can be considered as complementary variables with regard to their influence on the occurrence of hysteresis: an increase in temperature has qualitatively a similar effect as a decrease in pore size. Both lead to a decrease in the width of the hysteresis loop, which eventually disappears at certain critical pore size and temperature, which is illustrated in Figure 5.

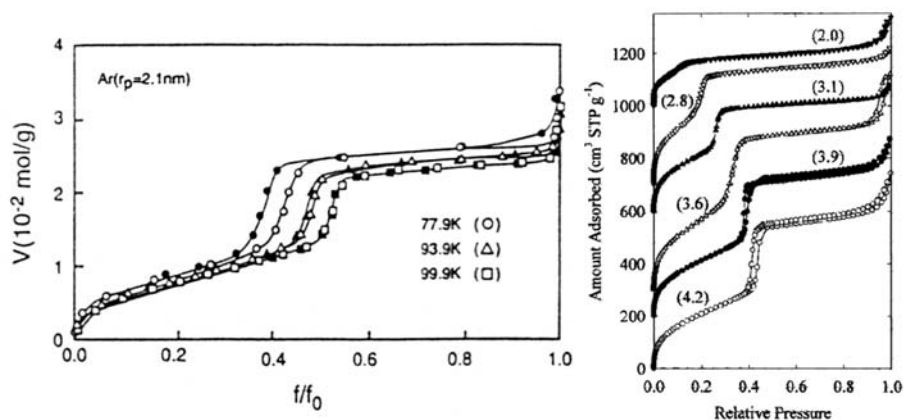


**Figure 5.** (a) Argon sorption as a function of temperature in a MCM-41 silica sample of pore radius 2.1 nm. From [76]. (b) Argon sorption at 87 K as a function of pore diameter in MCM-41 silica. From [116].

We can separate the following regimes: (i) Continuous pore filling without pore condensation step occurs below a certain critical pore width ( $W_c$ ), at a given temperature  $T < T_c$ . For a given pore size ( $W$ ) continuous pore filling can be observed above the pore critical temperature  $T_{wc}$  (and of course above the bulk critical temperature); (ii) Reversible pore condensation occurs for pore sizes between the critical pore size  $W_c$  and the pore size where hysteresis disappears ( $W_h$ ), i.e., in the pore size range  $W_c < W < W_h$ ; or in case of fixed pore size in the temperature range between the hysteresis critical temperature  $T_h$  and the pore critical temperature  $T_{wc}$ ; (iii) Pore condensation with hysteresis occurs for pore sizes larger than  $W_h$  (for a given pore size) and at temperatures below  $T_h$ .

In addition to the shift in critical temperature, experiments and theory indicate that as a result of the combined effects of fluid-wall forces and finite-size the freezing temperature and triple point of the pore fluid may also be shifted to lower temperature relative to the bulk triple point, if the wall-fluid attraction is not too strong, i.e., the pore wall does not prefer the solid phase [70]. Hence, pore condensation can be also observed at temperature below the bulk triple point temperature (an example is argon pore condensation at 77 K in mesoporous silica materials of diameters  $< 15 \text{ nm}$ , see figure 3b [20,44]). Theoretical and experimental studies have led to the conclusion that the complete coexistence curve of a fluid confined to mesoporous silica materials is shifted to lower temperature and higher mean density [71,73,75] (see also the review of Gelb et al [70]). Please note, that an elevation of the freezing temperature is however

observed in case of strong adsorption forces (e.g, cyclohexane adsorption in carbon pores [78]). Figure 6 shows the schematic phase diagrams of bulk- and pore fluid and illustrates the influence of confinement on the sorption and phase behavior as it can be found for instance in case of mesoporous silica.

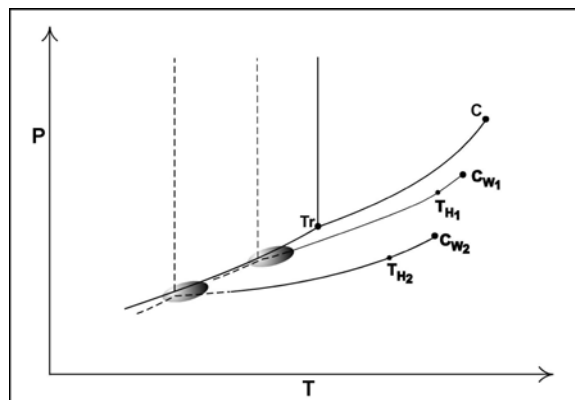


**Figure 6.** Schematic phase diagram of a bulk and pore fluid confined to different sized pores of widths  $W_1 > W_2$ . The pore condensation lines, i.e, the locus of states of the unsaturated vapour at which pore condensation will occur end in the appropriate pore critical points  $C_{w1}$  and  $C_{w2}$ , with  $T_{Cw1} > T_{Cw2}$ . For a given experimental temperature pore condensation will occur first in the pore of width  $W_2$ , and a higher (relative) pressure in the larger pore  $W_1$ . The temperatures  $T_{H1}$  and  $T_{H2}$  are the hysteresis critical temperatures, where experimental hysteresis disappears. Details of the sorption and phase behavior below the bulk triple point as well as the nature of pore triple points is still under investigation [20,48,70, 76, 78-83]. Hence, these regions of the phase diagram are indicated by dashed lines and the grey areas. (Please note, that from a theoretical point of view, real phase transitions and therefore real criticality cannot occur in pseudo-onedimensional cylindrical pores, i.e., pore condensation and the pore critical point should therefore be considered here as pseudo-phase transition and pseudo-critical point, respectively).

These observations reveal clearly that the shape of sorption isotherms does not depend only on the texture of the porous material, but also on the difference of thermodynamic states between the confined fluid and bulk fluid phase. This has to be taken into account for the characterization of porous media by gas adsorption, i.e., macroscopic, thermodynamic approaches based on the Kelvin equation, Broeckhoff and de Boer and Cole-Saam theories fail to predict correctly the influence of confinement on the phase and critical behavior of pore fluids. They are therefore inaccurate for pore size analysis in a temperature and pore size range

where hysteresis disappears, i.e., close to the hysteresis- and pore critical temperature (this will be discussed in more detail in section 4).

### 3.3 Pore condensation hysteresis

#### 3.3.1 IUPAC classification of hysteresis loops

It is widely accepted that there is a correlation between the shape of the hysteresis loop and the texture (e.g., pore size distribution, pore geometry, connectivity) of a mesoporous adsorbent. An empirical classification of hysteresis loops was given by the IUPAC [1], which is based on an earlier classification by de Boer [84]. The IUPAC classification is shown in figure 7. According to the IUPAC classification type H1 is often associated with porous materials consisting of well-defined cylindrical-like pore channels or agglomerates of compacts of approximately uniform spheres. It was found that materials that give rise to H2 hysteresis are often disordered and the distribution of pore size and shape is not well defined. Isotherms revealing type H3 hysteresis do not exhibit any limiting adsorption at high  $P/P_0$ , which is observed with non-rigid aggregates of plate-like particles giving rise to slit-shaped pores.

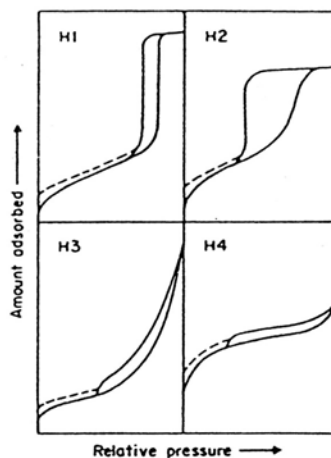


**Figure 7.** IUPAC classification of hysteresis loops. From [1].

The desorption branch for type H3 hysteresis contains also a steep region associated with a (forced) closure of the hysteresis loop, due to the so-called tensile strength effect. This phenomenon occurs for nitrogen at 77 K in the relative pressure range from 0.4 – 0.45 [52]. Similarly, type H4

loops are also often associated with narrow slit pores, but now including pores in the micropore region.

### 3.3.2 Origin of hysteresis

The mechanism and origin of sorption hysteresis is still under investigation. There are essentially three models which contribute to the understanding of sorption hysteresis: (i) *Independent (single) pore model*: Sorption hysteresis is considered as an intrinsic property of a phase transition in a single, idealized pore, reflecting the existence of metastable gas states. The hysteresis loop expected for this case is of type H1, according to the IUPAC classification [4]; (ii) *Network model*: Sorption hysteresis is explained as a consequence of the interconnectivity of a real porous network with a wide distribution of pore sizes. If network- and pore blocking effects are present a hysteresis loop of type H2 (IUPAC classification) is expected; (iii) *Hysteresis in disordered porous materials*: A more realistic picture takes into account that the thermodynamics of the pore fluid is determined by phenomena spanning the complete pore network: Hysteresis is here associated with thermodynamic metastability of low and high density phases of the pore fluid. In addition the occurrence of long time dynamics was suggested, which is so slow that on (experimentally) accessible time scales, the systems appear to be equilibrated. Typically, hysteresis loops of types H1 and H2 are observed in disordered porous materials.

Below we discuss the different models for hysteresis in more detail.

#### (a) Independent pore model

Different approaches, which would explain the occurrence of hysteresis in a single pore can be found in the literature since *ca.* 1900. Cohan [see refs. 52, 54] assumed that pore condensation occurs by filling the pore from the wall inward (for a cylindrical pore model). It was suggested that pore condensation would be controlled by a cylindrical meniscus once the pore is filled, whereas evaporation of the liquid would occur from a hemispherical meniscus, which would lead according to the Kelvin equation to different values of  $P/P_0$  for condensation and evaporation.

Theories by Foster [see ref. 52,54], Everett [86], Cole and Saam (CS) [65] and Ball and Evans [87] suggested that hysteresis may be caused by the development of metastable states of the pore fluids associated with the capillary condensation transition in a manner analogous to superheating or supercooling of a bulk fluid. Theoretical studies applying Non Local

Density Functional Theory (NLDFT) revealed that in principle both, pore condensation and pore evaporation can be associated with metastable states of the pore fluid [89]. This is consistent with the classical van der Waals picture, which predicts that the metastable adsorption branch terminates at a vapor-like spinodal, where the limit of stability for the metastable states is achieved and the fluid spontaneously condenses into a liquid-like state. Accordingly, the desorption branch would terminate at a liquid-like spinodal, which corresponds to spontaneous evaporation. In practice however, metastabilities occur only on the adsorption branch. Assuming a pore of finite length (which is always the case in real adsorbents) vaporization can occur via a receding meniscus, a nucleation problem and therefore metastability is not expected to occur during desorption (evaporation). This situation is illustrated in Figure 8 [89]. The NLDFT adsorption isotherm of Ar at 87 K in a cylindrical pore is shown in comparison with the appropriate experimental sorption isotherm on a MCM-41 silica material. Good agreement is obtained; however the small steps in the theoretical isotherm are a consequence of assuming a structureless (i.e., chemically and geometrically smooth) pore wall model, which neglects the heterogeneity of the MCM-41 pore walls.

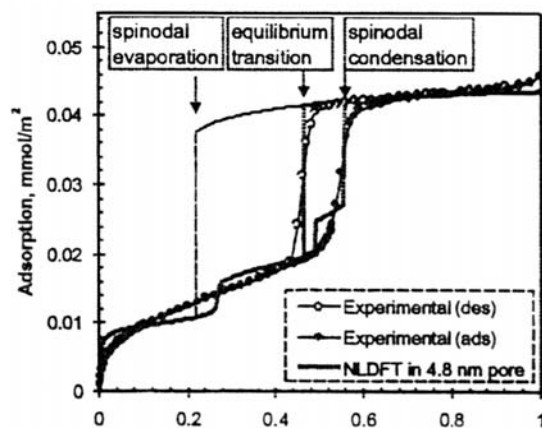


**Figure 8.** NLDFT adsorption isotherm of argon at 87 K in a cylindrical pore of diameter 4.8 nm in comparison with the appropriate experimental sorption isotherm on MCM-41. From [89].

It can be clearly seen, that the experimental desorption branch is associated with the equilibrium gas-liquid transition (the equilibrium transition corresponds to the condition at which the two states have equal grand

potential), whereas the condensation step corresponds to the spinodal spontaneous transition.

These results clearly indicate that the H1 hysteresis generally observed in MCM-41 material can be attributed to the occurrence of metastable states associated with the pore condensation transition (spinodal condensation). According to the situation described in figure 8, the desorption branch should be chosen for pore size analysis if theories/methods are applied, which describe the equilibrium transition (e.g., BJH, conventional NLDFT). In addition, Ravikovitch and Neimark developed recently a NLDFT based method, which correlates the location of the spinodal transition with the pore size [89], i.e., the model takes into account the existence of metastable states of the pore fluid. This method is accurate for pore sizes larger ca. 5 nm and can be applied to the adsorption branch. Application examples of this method for pore size analysis are given in section 4.2.

Hysteresis of type H1 is not only observed in materials consisting of independent cylindrical-like pores, this type of hysteresis can also be observed in ordered three dimensional pore systems such as MCM-48. Argon adsorption hysteresis of type H1 was found at 77.35 K for pore diameters larger than ca. 3.0 nm, and for argon adsorption at 87.27 K for materials of pore size larger than ca. 4.1 nm [20,48]. A combined analysis of a reversible nitrogen isotherm (at 77 K) with an hysteretic argon sorption isotherm (at 87 K) revealed clearly that – although MCM-48 consists of a unique, three dimensional pore network – hysteresis can be described within the independent pore model, and the desorption branch of the argon sorption hysteresis loop corresponds to the equilibrium transition. Hence, similar as in case of MCM-41 the desorption branch appears to be correlated with the pore diameter, if a method for pore size analysis is applied, which is based on the equilibrium liquid-gas phase transition (e.g., BJH, NLDFT).

Other materials consisting of ordered pore networks, as for instance controlled pore glasses and some types of sol-gel glasses also reveal H1 hysteresis loops. Awschalom et al [90] investigated the adsorption behavior of krypton (at 118 K) and oxygen (at 90 K) in highly ordered sol-gel porous glass. The remarkable oxygen isotherm, which reveals H1 hysteresis of almost vertical adsorption and desorption branches is shown in Figure 9. The data were analysed within the framework of the Saam-Cole (SC) theory [65]. In the Saam-Cole (SC) theory, pore condensation and the hysteresis connected with this transition is explained by considering the limits of stability and metastability of an adsorbed multilayer film in a cylindrical pore. The SC theory yields a map of

regions of stability, metastability, and instability in terms of the fluid-wall interaction parameter  $\alpha$ , surface tension  $\gamma$ , density difference  $\Delta\rho$  between gas and liquid. According to the SC theory, pore condensation occurs at a critical film thickness  $t_c$  (i.e.,  $a_c = r - t_c$ ;  $r$  is the pore radius) where the cylindrical adsorbed film becomes unstable. Evaporation occurs at lower  $P/P_0$  and the remaining film thickness is  $t_m$  (i.e.,  $a_m = r - t_m$ ). Hence, the range of metastable film thickness is given by the difference  $a_m - a_c$ .

The hysteresis of both, krypton and oxygen isotherms were in agreement with the predictions of the Saam-Cole theory (see figure 9), i.e., hysteresis is attributed to the existence of metastable pore fluid associated with pore condensation. This indicates again, that in ordered pore networks hysteresis can still be dominantly caused by the existence of metastable states. Accordingly, classical networking and pore blocking effects are not necessarily present in an interconnected pore system.

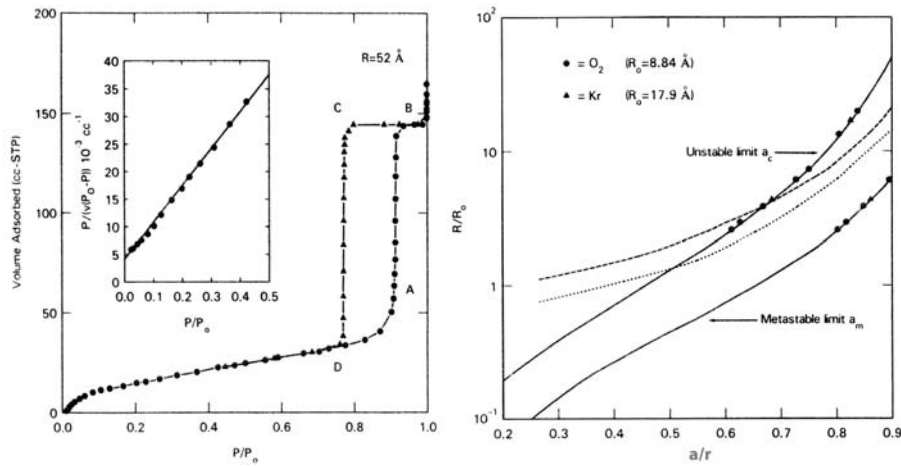


**Figure 9.** (a) Oxygen sorption isotherm at 90 K in highly ordered sol-gel porous glass of pore radius  $r = 52 \text{ \AA}$ . From [90]. (b) Comparison of the SC theory with experimental results. The solid lines represent the predictions of the SC theory for adsorbed film thickness at the relative pressures where pore condensation ( $a_c$ ) and evaporation ( $a_m$ ) occurs. The dependence of the unstable limit  $a_c/r$  and the metastable limit  $a_m/r$  is plotted in units of the dimensionless variables  $R_0$ , which is a scaling factor depending on details of the fluid-solid system (e.g., fluid-wall interaction parameter  $\alpha$ , surface tension  $\gamma$ , density difference  $\Delta\rho$  between gas and liquid). Dashed and dotted lines are Kelvin equation predictions for pore condensation and evaporation. From [90].

The applicability of the Cole-Saam theory has been tested in detail by Findenegg et al. based on sorption isotherms obtained with organic



vapours on controlled-pore glasses [128]. In this systematic experimental study some predictions of the SC theory could be confirmed.

(b) *Network model*

Network models take into account, that in many materials the pores are connected and form a three-dimensional network. An important feature of the network model is the possibility of pore blocking effects during evaporation, which occurs if a pore has access to the external gas phase only via narrow constrictions (e.g., an ink-bottle pore). The basis for the understanding of sorption hysteresis in ink-bottle pores and networks can be found in the work of McBain (see description in [52]). The wide inner portion of an ink-bottle pore is filled at high relative pressures, but it cannot empty during desorption until the narrow neck of a pore first empties at lower relative pressure. Thus, in a network of ink-bottle pores the capillary condensate in the pores is obstructed by liquid in the necks. The relative pressure at which a pore empties now depends on the size of the narrow neck, the connectivity of the network and the state of neighboring pores. Hence, the desorption branch of the hysteresis loops does here (in contrast to the single pore model) not occur at thermodynamic equilibrium, but reflects a percolation transition. In such a case the desorption branch of the hysteresis loop is much steeper as compared to the adsorption branch) leading to H2 hysteresis according to the IUPAC classification. Work by Everett [86] and others have led to the development of several specific network models. Advanced network or percolation models were introduced for instance by Mason [91] Wall and Brown [92], Neimark [93] Parlar and Yortsos [94], Ball and Evans [87], Seaton et al. [95] and Rojas et al. [96]. Page et al [97] suggested the existence of a percolation mechanism in case of the observed H2 hysteresis in porous vycor glass based on experimental results obtained by combining gravimetric and volumetric adsorption measurements with ultrasonic and optical measurements. Hoinkis et al [98] performed *in situ small angle* neutron scattering experiments in a disordered mesoporous silica glass (Gelsil 75). A H2 hysteresis loop was observed together with clear evidence of differences in the mechanisms of capillary condensation and evaporation, i.e., the latter was indicative of a percolation transition.

However, the existence of the conventional pore blocking mechanism as described above was recently questioned by Sarkisov and Monson [99]. They used molecular dynamics to study the adsorption and desorption of fluids in various simple geometries, including a simple ink-bottle pore geometry. Their data indicated clearly that the shape of the obtained H2 hysteresis loop was not caused by the occurrence of conventional pore blocking. The large

cavities could be emptied by a diffusional mass transport process from the fluid in the large cavity to the narrow neck and from there into the gas phase, hence the pore body can empty even while the pore neck remains filled.

A very recent experimental study of  $N_2$ , Ar and Kr at 77.4 and 87.4 K in ordered mesoporous materials with 3D cage-like structure (FDU-1 and SBA-16) combined with a NLDFT study (applying NLDFT) by Ravikovitch and Neimark focussed on a detailed description of the effect of an ink-bottle pore geometry on adsorption hysteresis. This work suggests that both, conventional pore blocking and cavitation (i.e., spinodal evaporation, see figure 5) can occur depending on temperature and pore size. The cavitation effect is correlated with the occurrence of a lower limit of hysteresis (classically described as the so-called tensile strength effect, which we will discuss in section 3.3.3).

### *(c) Pore condensation and hysteresis in disordered systems*

Even with the incorporation of network and percolation effects the adsorption thermodynamics is still modeled at a single pore level, i.e., the behavior of the fluid in the entire pore space is not assessed. In order to achieve this one needs to consider models which attempt to describe the microstructure of porous materials at length scales beyond that of a single pore. According to Gubbins et al. [100] there are two general approaches to construct a model of nanoporous materials by methods of molecular simulation. The first is the so-called mimetic simulation, and involves the development of a simulation strategy, that mimics the development of the pore structure in the materials preparation. The second approach is the reconstruction method. Here one seeks a molecular model, whose structure matches available experimental structure data. Monson and Co-workers investigated by Monte Carlo simulation the condensation and hysteresis phenomena of a Lennard Jones fluid in a reconstructed model of silica xerogel [101]. Their adsorption isotherms exhibited hysteresis loops of type H1 and H2 in agreement with experimental results obtained on the same type of material. The observed hysteresis was attributed to thermodynamic metastability of the low and high density phases of the adsorbed fluid – however these phases span the entire void space of the porous material and are therefore not associated with the individual pores. Pellenq et al [102] studied the pore condensation and hysteresis behavior of argon in a pseudo-vycor glass, which was obtained by a off-lattice reconstruction method over a wide temperature range via Monte Carlo simulation. Hysteresis loops of type H2 were observed; the steep

evaporation/desorption branch was associated with a first-order phase transition in a disordered system (no pore blocking effects were invoked).

Gelb and Gubbins [103,104] have recently reproduced the complex network structure of porous glasses such as vycor and controlled-pore glass by applying molecular simulation. Grand Canonical Monte Carlo simulation results for xenon adsorption in these pores suggest strongly that the shape of the adsorption/desorption hysteresis does not depend on the connectivity of the material model, supporting the hypothesis that in materials of this type (e.g., a porous Vycor glass with a porosity of 30%) the fluid in different pores behaves quasi-independently, and that no system-spanning phase transitions occur during adsorption or desorption [104]. The origin of hysteresis in disordered porous glasses was recently also investigated by lattice DFT models [105] and Monte Carlo simulations [106]. These studies indicate that hysteresis is due to the presence of a large number of metastable states. It was concluded that the origin of the hysteresis is associated with long time dynamics, which is so slow that on (experimentally) accessible time scales, the systems appear to be equilibrated, which leads to the observed reproducible results in the observation of the hysteresis loop.

These results discussed above indicate that the nature of hysteresis in disordered systems is very complex. More theoretical and experimental work is necessary to (i) clarify what determines the shape of the hysteresis loop in such disordered systems to be H2 and (ii) to obtain a clearer picture of the nature of phase and also critical behavior of fluids in disordered porous systems.

### *3.3.3 Lower limit of the hysteresis loop - tensile strength hypothesis*

It was observed already a long time ago, that the hysteresis loop for nitrogen adsorption at 77.35 K closed at relative pressure at or above 0.42, apparently independent of the porous material (see [54]). Experimental results with other adsorptives also supported the view, that for a given temperature this lower closure point of hysteresis is never located below a certain critical relative pressure. It was suggested that the lower closure point of hysteresis is determined by the tensile strength of the capillary condensed liquid, i.e., there exists a mechanical stability limit below which a macroscopic meniscus cannot exist anymore and which leads to a spontaneous evaporation of the pore liquid. This is in contrast to the situation of pore blocking where the evaporation of the liquid is controlled by the necks of the ink-bottle pores. The tensile strength theory was analysed by Burgess and Everett [107] and very recently by Sonwane and

Bhatia [108], Ravikovich and Neimark [109], as well as by Findenegg et al [110]. Based on an extensive theoretical (by NLDFT) and experimental studies on capillary condensation of  $N_2$ , Ar and Kr in materials with well defined ink-bottle pores (SBA-16, and FDU-1) Neimark and Ravikovitch found that the lower limit of the hysteresis loop also depends on the pore geometry, which questions the conventional assumption, that the lower limit of the hysteresis loop is a unique function of the adsorbate and the temperature.

Findenegg et al. [110] performed a systematic experimental study of the pore condensation hysteresis of  $CHF_3$  and  $C_2F_6$  in mesoporous silica with open cylindrical pores of uniform size (MCM-41 and SBA-15) and in a silica material consisting of large cellular mesopores, which are accessible only via narrow mesopores (which resembles an ink-bottle geometry). Their sorption results show that the lower closure point of hysteresis observed in the materials with ink-bottle geometry and the pore condensation pressure observed at the hysteresis critical temperature (i.e., the temperature at which hysteresis disappears) for the sorption isotherms in ordered MCM-41 and SBA-15 almost coincide. Hence, there appears to be a relation between the lower closure point of the hysteresis loop and the hysteresis critical temperature in uniform cylindrical pores. A correlation between the lower closure point of hysteresis and the hysteresis critical temperature was also suggested by Bhatia et al. [108].

Despite the fact, that the occurrence of the lower closure point of hysteresis is still not sufficiently understood, it is clear that it leads to a problem for pore size calculations. The existence of a lower closure point affects primarily the position of the desorption branch with regard to its position and steepness, i.e., the desorption isotherm exhibits a characteristic step at the lower closure point. Hence a pore size calculation based on an analysis of the desorption branch is here not straightforward.

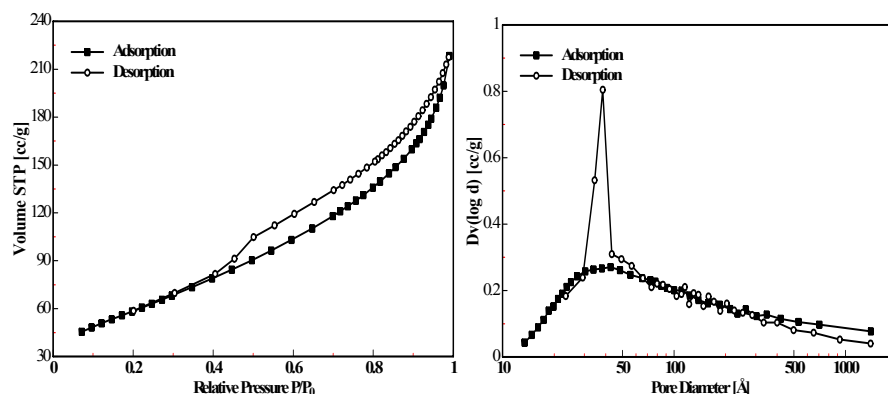


**Figure 10.** Nitrogen adsorption/desorption at 77.35 K on a disordered alumina catalyst and BJH pore size distribution curves from adsorption and desorption branches.

A typical example is given in Figure 10, which shows nitrogen sorption data on a highly disordered alumina catalyst sample together with BJH pore size distribution curves obtained from both, adsorption and desorption branches. As it can be clearly seen the hysteresis loop closes at a relative pressure of ca. 0.4-0.45 and exhibits the mentioned characteristic step down. This step is not associated with the evaporation of pore liquid from a specific group of pores, i.e., the spike in the desorption pore size distribution curve (PSD) reflects an artifact, caused by the spontaneous evaporation of metastable pore liquid (cavitation, i.e., the tensile strength effect). In contrast, the PSD derived from the adsorption branch does not reveal this artificial peak and represents the wide pore size distribution curve, which is characteristic for such an disordered sample.

#### 4 Pore size analysis of mesoporous solids

##### 4.1 Classical, macroscopic thermodynamic methods versus microscopic models (NLDFT) for pore size analysis

Among the classical methods for mesopore size analysis, the method of Barrett-Joyner-Halenda (BJH), which was proposed in 1951 is certainly the most popular one. The BJH-approach provides an algorithm to calculate the pore size distribution (PSD) by assuming a cylindrical pore geometry from nitrogen desorption data (obtained at 77.35 K). The BJH-approach attracted much attention and was later modified by Dollimore and Heal, Cranston-Inkley [52,53] and others.

All methods related to the original BJH approach are based on the modified Kelvin equation and the accuracy of the calculated PSD depends on the applicability and the deficiencies of the Kelvin equation, which were already discussed to some extent in sections 3.1 and 3.2. In narrow pores attractive fluid-wall interactions are dominant and the macroscopic, thermodynamic concept of a smooth liquid-vapor interface and bulk-like core fluid cannot realistically be applied. In addition, methods based on the modified Kelvin equation do not take into account the influence of the adsorption potential on the position of the pore condensation transition. It is further assumed that the pore fluid has essentially the same thermophysical properties as the correspondent bulk fluid. For instance, the surface tension of the pore liquid is thought to be equal to the properties of the corresponding bulk liquid, but the surface tension of the pore liquid depends on the radius of curvature. Significant deviations from the bulk surface tension are however expected to occur in narrow mesopores [52,55, 111]. Another problem is that the thickness of the preadsorbed multilayer film is assessed by the statistical thickness of an adsorbed film on a nonporous solid of a surface similar to that of the sample under consideration. However, in particular for narrow pores of widths  $< \text{ca.} 10 \text{ nm}$  this mean thickness does not reflect the real thickness of the preadsorbed multilayer film, because curvature effects are not taken into account.

A direct experimental test of the validity of the Kelvin equation and its modifications became possible (as indicated before) after mesoporous molecular sieves became available, where the pore diameter could be derived by independent methods (such as x-ray-diffraction, high resolution transmission electronic microscopy). It is found that the BJH- and related approaches based on the modified Kelvin equation underestimate the pore size up to 25 % for pores smaller than 10 nm.

Corrections of the modified Kelvin equation in the spirit of the Broeckhoff de Boer and Cole-Saam approach were for instance developed by Lu et al. [111], Lukens et al. [38], Galarneau et al [56], Bhatia et al.[112], Groen et al [113]. These modified classical models were tested using MCM-41 and/or SBA-15 materials in combination with pore size data derived from the aforementioned independent experimental methods. In general good agreement, but only over a limited pore size range was found. An empirical approach, which is meanwhile widely used was proposed by Kruk, Jaroniec and Sayari (KJS) [36,114]. This method is based on a corrected (modified) BJH equation, which was properly *calibrated* using MCM-41 mesoporous silica materials. Series of MCM-41 silicas of cylindrical pores of size between 2 and ca. 7 nm were originally

used to establish a relation between capillary condensation/evaporation pressures and pore size. A pore size assessment independent from the pore condensation pressure could be obtained from XRD interplanar spacing and the primary mesopore volume. The KJS approach is strictly valid only for MCM-41 type silica materials over a pore size range which reflects the range over which a calibration curve exists (i.e., meanwhile 2 – ca. 12 nm), however the KJS-approach tends to overestimate the pore size for diameters  $> 8$  nm [110]. The method is meanwhile also available for argon adsorption in MCM-41 silica at 87.27 K [116] and 77.35 K [117], as well as for the analysis of hydrophobized mesoporous solids [118].

In contrast to the Kelvin equation based methods, microscopic methods based on Density Functional Theory [119-125] and the Grand Canonical Monte Carlo simulation (GCMC) [68,69] methods correctly describe the local fluid structure near curved solid walls on a microscopic level. These methods also capture correctly (as discussed before in section 3.2) that the thermodynamics of the confined fluid is altered as compared to the bulk fluid (e.g., critical point shifts) and consequently that pore condensation and hysteresis disappear already below the so-called hysteresis critical temperature and for pore sizes below a certain critical pore width. This is important for an accurate pore size analysis of narrow mesopores. Because the equilibrium density profiles are known for each pressure along an isotherm (i.e., these isotherms are calculated by integrating of the equilibrium density profiles,  $\rho(r)$ , of the fluid in the model pores) no assumptions about the pore filling mechanism are required as in case of the macroscopic methods. As a consequence these microscopic methods can be applied for pore size analysis over a large range of pore widths, i.e., from micropores up to well into the meso-macropore range. It is a general practice to adjust interaction parameters (fluid-fluid and fluid-solid) in such a way that the model would correctly reproduce fluid bulk properties (e.g., bulk liquid-gas equilibrium densities and pressures, liquid-gas interfacial tensions) as well as standard adsorption isotherms on well-defined non-porous adsorbents. A set of isotherms calculated for a set of pore sizes in a given range for a given adsorbate constitutes a model database, which is called a so-called kernel.

The calculation of pore size distribution is based on a solution of the Generalized Adsorption Isotherm Equation (GAI), which correlates the kernel of theoretical adsorption/desorption isotherms with the experimental sorption isotherm:

$$N(P/P_0) = \int_{W_{MIN}}^{W_{MAX}} N(P/P_0, W) f(W) dW \quad (6)$$

where,  $N(P/P_0)$  = experimental sorption isotherm data,  $W$  = pore width

$N(P/P_0, W)$  = theoretical sorption isotherm on a single pore of width  $W$

$f(W)$  = pore size distribution function.

The GAI equation reflects the assumption that the total isotherm consists of a number of individual single pore isotherms multiplied by their relative distribution,  $f(W)$ , over a range of pore sizes. The set of  $N(P/P_0, W)$  isotherms (kernel) for a given system (adsorptive/adsorbent) can be obtained, as indicated above, by either Density Functional Theory or by Monte Carlo computer simulation. The pore size distribution is then derived by solving the GAI equation numerically. In general, the solution of the GAI represents an ill-posed problem, which requires some degree of regularization. However, existing regularization algorithms allow to obtain meaningful and stable solutions of the GAI equation [ 89 ]

Figures 11 [126] and 12 [127] compare the predictions of various methods such as BJH, 4V/S (i.e, pore volume determined by Gurvitch rule,  $S$  is the BET surface area), Broeckhoff and de Boer (BDB), and DFT for the pore size analysis of MCM-41 and SBA-15 samples with pore diameters determined by experimental methods which are independent of the position of the pore condensation/evaporation steps of adsorption isotherms (e.g., XRD +  $V_{\text{meso}}$ ). The data displayed in figure 11 reveal that both the DFT and BDB method agree quite well with the pore size values obtained from the independent method, whereas the BJH results clearly disagree. Figure 12 shows clearly, that over the complete pore size range good agreement exists between the experimental pore sizes and the ones determined by NLDFT from adsorption and desorption branch. It is also visible, that the BJH method significantly underestimates the pore sizes over a wide pore diameter range. Again, better agreement is obtained with methods based on the Broeckhoff and de Boer approach. However, significant deviations between the BDB- and NLDFT methods occur for pore diameters  $< 7$  nm [126], mainly due to the fact that the Broeckhoff and de Boer method cannot predict the existence of pore criticality and the associated disappearance of sorption hysteresis below a certain critical pore diameter at given temperature (see section 3.2).



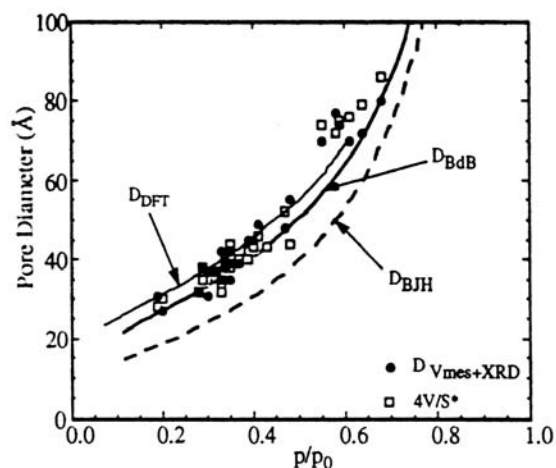


**Figure 11.** Pore size dependence of the relative pressure of evaporation (desorption) of nitrogen in MCM-41: Comparison of predictions of BJH, BdB and DFT with experimental pore size data ( $4V/S$ ,  $D_{Vmes} + XRD$ ). From [126].

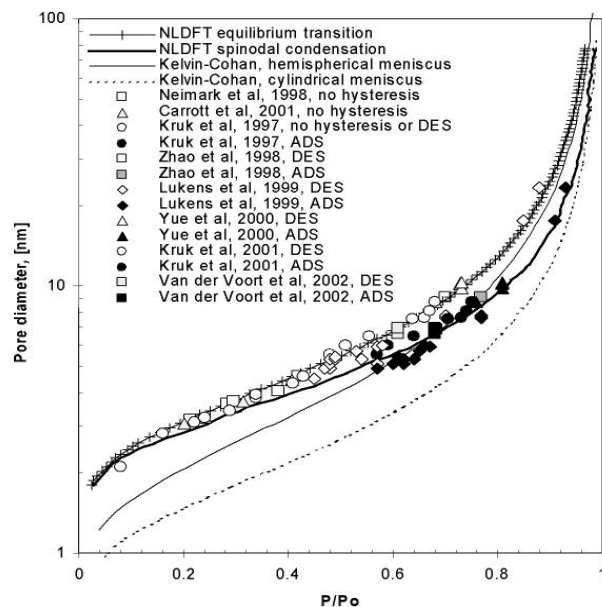


**Figure 12.** Pore size dependence of the relative pressure of condensation and evaporation for  $N_2$  in cylindrical pores: Comparison of theoretical predictions (NLDFT- and BJH (Kelvin-Cohan) with experimental pore size data for MCM-41 and SBA 15. From [127].

#### 4.2 Use of the adsorption or desorption branch for pore size calculation?

The presence of the hysteresis loop introduces a considerable complication, and of course the question arises whether the adsorption branch or the desorption branch of a hysteretic sorption isotherm should be used for the pore size analysis. The answer of this question depends on the texture of the adsorbent, and in case of highly disordered systems, where the nature of hysteresis is very complex, it might be even impossible to correlate the adsorption or the desorption branch of the hysteresis loop with the true pore size and pore size distribution. In the following we discuss the question whether the adsorption or desorption branch should be used for pore size calculations based on our discussion of the origin of hysteresis in section 3 of this review. However, the nature of hysteresis is still under investigation and a general agreement could not even be reached for simple systems. Hence, our conclusions have therefore to be considered as to be preliminary.

In case of ordered materials such as MCM-41 and SBA-15 a lot of progress was made with regard to the understanding of the nature of pore condensation and hysteresis. The typically observed H1 hysteresis can be modeled by the independent pore model (see section 3.3.2). Hysteresis can here be attributed to the occurrence of metastable states of the pore fluid associated with pore condensation. It is believed that the desorption branch of the hysteresis loop reflects the equilibrium phase transition, i.e., theories and methods which describe the equilibrium phase transition (e.g., BJH, NLDFT etc..) should be applied to the desorption branch in order to calculate the pore size correctly. The adsorption branch can also be taken for pore size analysis if a theory (method) is applied which takes metastability into account and provides a correlation between the relative pressure where spinodal condensation occurs and the pore size. As mentioned before (section 3.3) such a method, based on NLDFT (*NLDFT-spinodal condensation method*), was suggested by Ravikovitch and Neimark [89]. Another possibility is to apply an empirical method such as the KJS approach [36], which however can only be applied for pore size analysis over a limited pore size range, i.e., the range over which a kind of calibration curve exists, which represents a correlation between the pore size and the pore condensation pressure.

The situation is more complex for materials consisting of a three-dimensional network of pores. Based on our discussion in section 3.32(a) it appears that pore condensation hysteresis of type H1 as observed in

ordered three dimensional pore systems (e.g. MCM-48, some ordered sol-gel glasses, CPG) is still dominantly caused by metastabilities associated with the pore condensation transition. Also here it is believed that the desorption branch of the hysteresis loop can be associated with the equilibrium gas-liquid phase transition, i.e., the desorption branch should be chosen for pore size analysis if theories/methods are applied which are based on the equilibrium transition (e.g., BJH, equilibrium transition NLDFT, see also section 3.3.2.a).

In case of highly disordered materials (e.g., porous vycor glass), the occurrence of hysteresis is as discussed before in section 3.3 associated with a variety of effects including metastable states of the pore fluid, potential pore blocking and percolation phenomena, effects from possible system-spanning transitions, long time dynamics etc. The significance of each mechanism for the shape of hysteresis depends on details of the texture of the porous material. Very often sorption hysteresis of type H2 is observed in such cases. In contrast to the situation in ordered materials, the desorption branch of the hysteresis loops can then not be used for pore size analysis by methods based on the equilibrium transition (e.g. BJH). This is also true if the evaporation of the pore liquid is caused by cavitation, i.e., evaporation occurs close to the lower limit of hysteresis as observed for instance in materials, which give rise to type H3 hysteresis (see Figure 10 in section 3.3.3 and discussion of so-called tensile strength effect). Here a more realistic pore size analysis can be obtained from an analysis of the adsorption branch. Again, the application of empirical methods based on experimental calibration (e.g., KJS approach [36]) is certainly a good way to assess the pore size, but a pore size analysis over the complete mesopore range can be performed by applying the *NLDFT-spinodal condensation method* [89].

It was further suggested to check the consistency of the pore size analysis by applying the conventional NLDFT method (describing the equilibrium condensation/evaporation transition) to the desorption branch and the NLDFT-spinodal condensation method to the adsorption data [89]. This allows to compare theoretical and experimental “widths” of the hysteresis loops. Hysteresis loops, which are wider than those predicted theoretically (i.e., the pore size distribution curves calculated from adsorption and desorption branch do not agree), indicate that hysteresis cannot be solely explained within the framework of the independent pore model (see section 3.3.2.(a)).

We applied this approach on nitrogen data obtained at 77 K on ordered SBA-15, controlled-pore glass (CPG) and porous vycor glass (which can be considered as a disordered system compared to SBA-15). The results

are shown in Figures 13 – 15. The observed hysteresis loops for SBA-15 as well as for controlled pore glass are of type H1, whereas the porous vycor glass clearly exhibits type H2 hysteresis. The pore size distribution curves obtained from the adsorption branch (by applying the NLDFT-spinodal condensation method) and desorption branch (by applying the NLDFT equilibrium method) are in perfect agreement for SBA-15. This confirms that sorption hysteresis in this SBA-15 silica sample is caused by delayed condensation (i.e., by metastable states of the pore fluid occurring during adsorption/condensation). Good agreement between the PSD's calculated from the adsorption and desorption branches can also be found for the controlled-pore glass sample. Although controlled-pore glasses consist of a network of cylindrical-like pores, the hysteresis appears to be mainly due to metastability effects, i.e., the observed hysteresis can be described to a large extent by applying the independent pore model. This conclusion is partially in agreement with results obtained by Findenegg et al, who applied the Saam-Cole theory to describe the H1 hysteresis observed for the adsorption of organic vapors in controlled-pore glasses [128]. Here, a semi-quantitative agreement with theoretical prediction of the Saam-Cole theory could be obtained.

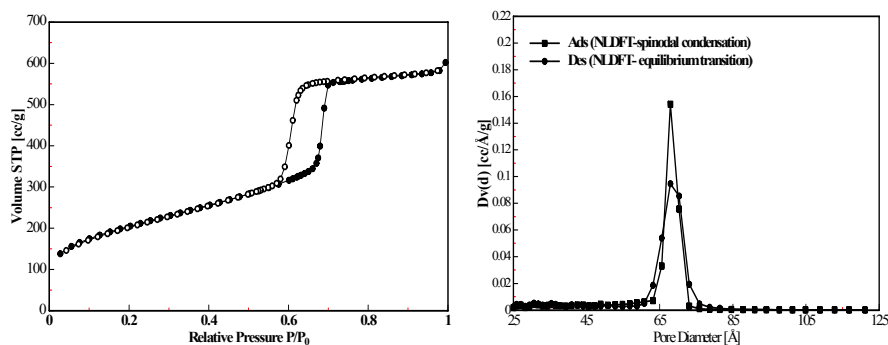


**Figure 13.** N<sub>2</sub> adsorption/desorption at 77 K in SBA-15 and pore size distributions from adsorption and desorption by applying NLDFT methods dedicated to describe the pore (spinodal) condensation (adsorption branch) and the equilibrium evaporation (desorption branch) transitions.

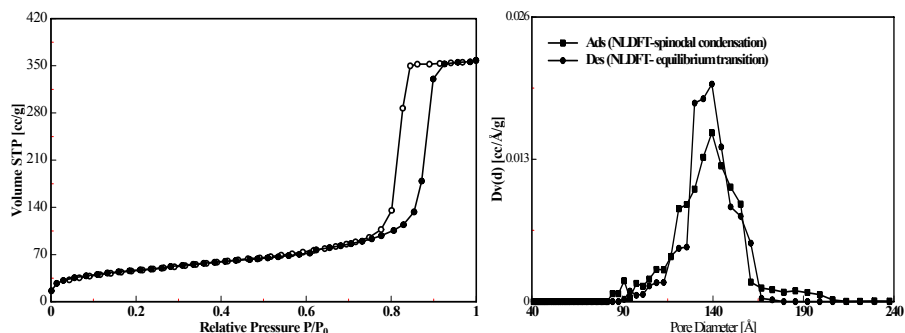


**Figure 14.**  $N_2$  adsorption/desorption at 77 K in controlled pore glass and pore size distributions from adsorption and desorption branch by applying NLDFT methods dedicated to describe the pore (spinodal)condensation (adsorption branch) and the equilibrium evaporation (desorption branch) transitions.

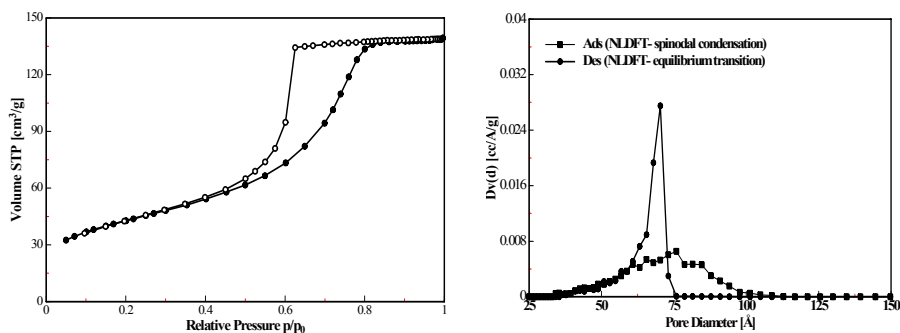


**Figure 15.** Nitrogen adsorption/desorption at 77 K in porous vycor glass and pore size distributions from adsorption and desorption branch by applying NLDFT methods dedicated to describe the pore (spinodal) condensation (adsorption branch) and the equilibrium evaporation (desorption branch) transitions.

However, the situation is different for the vycor glass sample. The pore size distribution obtained from the desorption branch is artificially sharp leading to the observed H2 type hysteresis. The disagreement between the pore size distribution curves obtained from adsorption and desorption branch indicates that hysteresis cannot be described within the single pore model. The mechanism of pore condensation and hysteresis in

vycor is in contrast to controlled pore glass much more complex and not fully understood (see section again sections 3.3.2 and 3.3.3). The observed H2 hysteresis in porous vycor is often attributed to the occurrence of pore blocking and percolation phenomena [e.g., 87,91,97], which however do not occur during adsorption (i.e. condensation). Hence, the pore size distribution calculated from the adsorption branch can here be considered as to be more realistic.

The examples discussed here and in section 3.3 confirm that the IUPAC classification of hysteresis loops can be in principle quite helpful to determine the “correct” branch of the hysteresis loop for pore size analysis. It seems that in ordered system very often H1 hysteresis occurs, whereas H2 and H3 hysteresis is typically observed for disordered mesoporous systems. There is some evidence that in many cases where type H1 hysteresis occurs – even if observed in materials consisting of three dimensional pore networks - the desorption branch is correlated with the equilibrium phase transition, and therefore with the pore size if methods based on the determination of the gas-liquid phase transition (e.g., BJH, equilibrium-NLDFT) are applied for pore size analysis. This is not the case for H2 and H3 hysteresis, and the analysis of the adsorption branch by applying a proper method (e.g., NLDFT-spinodal condensation method or Kelvin equation based approach calibrated for adsorption branch) may lead here to a more accurate pore size analysis.

However, it should be clearly stated, that the suggestions given above are certainly not justified for highly disordered materials, where a clear decision with regard to the type of hysteresis loop is not always possible. In such cases it is very helpful to include in the sorption experiment the measurement of so-called scanning curves (of the hysteresis loop), which allow to reveal details of the mechanisms of pore condensation and evaporation (e.g., effects of connectivity, existence of cooperative processes etc.) [86, 87,96]. In addition, the factors which determine the shape of the hysteresis loop are still not completely known for disordered, connected pore systems (see section 3.3.2). For instance, theoretical studies reveal the occurrence of H2 hysteresis without the implementation of pore blocking and percolation effects [105,106]. More work is needed to correlate such theoretical predictions with sorption experiments on disordered porous materials, where the texture can be explored by independent methods (e.g., SANS, SAXS [129]).

## **5 Concluding Remarks**

Significant progress was achieved during recent years with regard to the understanding of sorption phenomena in narrow pores. The shape of sorption isotherms depends on pore size and temperature (which reflects differences in the thermodynamic states of the pore fluid and the bulk fluid) and on the chemical and geometrical heterogeneity (i.e. the degree of disorder) of the porous material. These factors have to be taken into account in order to obtain a comprehensive and accurate pore size characteristics from the analysis of sorption isotherms. From an experimental point of view, nitrogen sorption at liquid nitrogen temperature (77 K) and argon sorption at liquid argon temperature (87 K) can be used to obtain a pore size analysis over the complete range of micro- and mesopores. In contrast, pore size analysis with argon at 77 K is limited to pores of diameters smaller than ca. 15 nm.

Major improvements with regard to the pore size analysis of mesoporous materials could be achieved mainly because of the following reasons: (i) the discovery of novel ordered mesoporous materials, such as MCM-41, MCM-48, SBA-15, which exhibit a uniform pore structure and morphology and can therefore be used as model adsorbents to test theories of gas adsorption; (ii) carefully performed sorption experiments; (iii) the development of microscopic methods, such as the Non-Local-Density Functional Theory (NLDFT) or computer simulation methods, which allow to describe the configuration of adsorbed molecules in narrow pores on a molecular level. These methods allow to obtain an accurate pore size analysis over a wide pore size (i.e., combined micro/mesopore analysis). In contrast, classical methods based on macroscopic thermodynamic assumptions (e.g., BJH) underestimate the pore size up to 25 % (for pore sizes < 10 nm), if not properly corrected or calibrated. Microscopic methods for pore size analysis take into account details of the fluid-fluid interactions and the adsorption potential (which depends on the strength of the fluid-wall interactions and the pore geometry). However, appropriate methods for pore size analysis based on NLDFT and GCMC are meanwhile available for many important fluid/substrate systems.

Despite this progress, a satisfying verification of theoretical models for the pore size analysis of mesoporous materials could be achieved so far only for highly ordered materials (such as mesoporous molecular sieves), which can be modeled within the framework of an independent pore model. It is found that methods and theories based on a single pore model are in some cases applicable (to some extent) to describe the sorption and phase behavior of fluids in porous materials consisting of

ordered three-dimensional pore networks. However, the phase and hysteresis behavior of fluids in disordered porous systems is still not well understood and more theoretical and experimental work is clearly required to understand the combined effects of confinement, pore geometry, connectivity, etc. on the origin of pore condensation and hysteresis. Furthermore, more work is necessary to evaluate to which extent pore size analysis in terms of a pore size distribution curve (which is essentially based on the single pore model) is appropriate in order to characterize materials consisting of complex, disordered pore networks. Therefore, it is important to develop more realistic adsorbent models, which attempt to describe the microstructure of porous materials at length scales beyond that of a single pore model. Predictions of such advanced models should be evaluated in combination with carefully performed sorption experiments.

## 6 Acknowledgements

The author would like to thank R. Ahmad for his help with the sorption experiments and R. Swinson for his support in the preparation of the graphics. Helpful discussions with J. Jagiello, S. Lowell and M.A. Thomas are gratefully acknowledged.

## 7 References

1. Sing K.S.W., Everett D.H., Haul R.A.W., Mouscou L., Pierotti R. A., Rouquerol J. and Siemieniowska T., Reporting physisorption data for gas/solid systems with special reference to the determination of surface area and porosity, *Pure & Appl. Chem.* **57** (1985) pp. 603 – 619.
2. Kresge C.T., Leonowicz M.E., Roth W.J., Vartuli J.C. and Beck J.S., Ordered mesoporous molecular sieves synthesized by a liquid-crystal template mechanism, *Nature* **359** (1992) pp. 710-712.
3. Zhao X S., Lu G.Q. (Max) and Millar J. G., Advances in mesoporous molecular sieve MCM-41, *Ind.Eng.Chem. Res.* **35** (1996) pp. 2075-2090.
4. Linden M., Schacht S., Schueth F., Steel A. and Unger K., Recent advances in nano- and macroscale control of hexagonal, mesoporous materials, *Journal of Porous Materials* **5** (1998) pp. 177 – 193.
5. Yanagisawa T., Schimizu T., Kuroda K. and Kato C., The preparation of alkyltrimethylammonium-kanemite complexes and their conversion to mesoporous materials, *Bull. Chem. Soc. Jpn.* **63** (1990) pp. 988-992.
6. Inagaki S., Fukushima Y. and Kuroda K., Synthesis of highly ordered mesoporous materials from a layered polysilicate, *J. Chem. Soc. Chem Commun.* **22** (1993) pp. 680- 682.



7. Zhao D.Y., Feng J.L., Huo Q.S., Melosh N., Frederickson G., Chemelka B.F. and Stucky G.D., Triblock copolymer syntheses of mesoporous silica with periodic 50 to 300 angstrom pores, *Science* **279** (1998) pp. 548 – 552.
8. Ryoo R., Ko C.H., Kruk M., Antochuk V. and Jaroniec M., Block-Copolymer-Templated Ordered Mesoporous Silica: Array of Uniform Mesopores or Mesopore-Micropore Network? *J. Phys. Chem B* **104** (2000) pp. 11465 -11471.
9. Galarneau A., Cambon H., Martin T., De Menorval L. C., Brunel D. and Di Renzo Fajula F., SBA-15 versus MCM-41: Are they the same materials?, *Studies in Surface Science and Catalysis* **141** (2002) pp. 395-402.
10. Barton T.J., Bull M., Klemperer W.G., Loy D.A., McEnaney B., Misono M., Monson P.A., Pez G., Scherer G.W., Vartuli J.C. and Yagi M. O., Tailored porous materials, *Chem Mater.* **11** (1999) pp. 2633-2656.
11. Moeller K. and Bein T., Inclusion chemistry in periodic mesoporous hosts, *Chem Mater.* **10** (1998) pp. 2950 – 2963.
12. Fröba M., Köhn K., Bouffaud B., Richard O. and Tendeloo G.V., Iron (III) oxide within mesoporous MCM-48 silica phases: Synthesis and Characterization, *Mat. Res. Soc. Symp. Proc.* (1999) pp. 547- 552.
13. Inagaki S., Guan Y., Fukushima Y., Oshuna T., and Terasaki O., Novel mesoporous materials with a uniform distribution of organic groups and inorganic oxide in their frameworks, *J. Am. Chem. Soc.* **121** (1999) pp. 9611-9614.
14. Sefa T., Ozin G., Grondy H., Kruk M. and Jaroniec M., Recent developments in the synthesis and chemistry of periodic mesoporous organosilicas, *Studies in Surface Science and Catalysis* **141** (2002) p. 1.
15. Muth O., Schellbach C. and Froeba M., Triblock copolymer assisted synthesis of periodic mesoporous organosilicas (PMOs) with large pores, *Chem. Commun.* (2001) pp. 2032 – 2033.
16. Jun S., Joo S, Ryoo R., Kruk M, Jaroniec M, Liu Z., Ohsuna T. and Terasaki O., Synthesis of new, nanoporous carbon with hexagonally ordered mesostructure, *J.Am.Chem.Soc.* **122** (2000) pp. 10712-10713.
17. Joo S.H., Ryoo R., Kruk M. and Jaroniec M., Evidence for general nature of pore interconnectivity in 2-dimensional hexagonal mesoporous silicas prepared using block copolymer templates, *J. Phys. Chem. B* **106** (2002) p. 4640.
18. Eddaoudi M., Li Hailian and Yagi O.M., Highly porous and stable metal-organic frameworks: structure design and sorption properties, *J. Am. Chem. Soc.* **122** (2000) pp. 1391 – 1397.
19. Murata K., Kaneko K., Kokai F., Takahashi K., Yudasaka M. and Ijima S., Pore structure of single-wall carbon nanohorn aggregates, *Chemical Physics Letters* **331** (2000) pp. 14-20.
20. Thommes M., Koehn R. and Froeba M., Sorption and pore condensation behavior of pure fluids in mesoporous MCM-48 silica, MCM-41 silica, SBA-15 silica and controlled-pore glass at temperatures above and below the bulk triple point, *Applied Surface Science* **196** (2002) pp. 239-249.
21. Rouquerol J., Avnir D., Fairbridge C.W., Everett D.H., Haynes J.H., Pernicone N., Ramsay J.D.F. and Sing K.S.W., Unger K.K., Recommendations for the characterization of porous solids, *Pure & Appl. Chem.* **66** (1994) pp. 1739 -1748.
22. Keller J.U. and Robens E., du Fresne von Hohenesche, Thermogravimetric and Sorption Measurement Techniques/Instruments, *Studies in Surface Science and Catalysis* **144** (2002) pp. 387 – 394.

23. Kaneko K., Determination of pore size and pore size distribution 1. Adsorbents and catalysts, *Journal of Membrane Science* **96** (1994) pp. 59-89.
24. Kaneko K., Ohba T., Hattori Y., Sunaga M., Tanaka H. and Kanoh H., Role of gas adsorption in nanopore characterization, *Studies in Surface Science and Catalysis* **144** (2002) pp. 11 -18.
25. Chenite A., Le Page Y. and Sayari A., Direct TEM imaging of tubules in calcined MCM-41 type mesoporous materials, *Chem Mater.* **7** (1995) pp. 1015-1019.
26. Franke O., Schulz-Ekloff, G., Rathousky J., Starek J. and Zukal A., Unusual type of adsorption isotherm describing capillary condensation without hysteresis, *J. Chem. Soc., Chem. Commun.* (1993) pp. 724-726.
27. Branton P.J., Hall P.G. and Sing K.S.W., Physisorption of nitrogen and oxygen by MCM-41, a model mesoporous adsorbent, *J. Chem. Soc Chem. Commun.* (1993) pp. 1257-1258.
28. <sup>a</sup> Rathousky J., Zukal A., Franke O. and Schulz-Ekloff G., Adsorption on MCM-41 mesoporous molecular sieve, Part I. Nitrogen isotherms and parameters of the porous structure, *J. Chem Soc. Faraday Trans.* **90** (1994) pp. 2821 -2826; <sup>b</sup> Rathousky J., Zukal A., Franke O. and Schulz-Ekloff G., Adsorption on MCM-41 mesoporous molecular sieve, Part II, Cyclopentane isotherm and their temperature dependence, *J. Chem. Soc. Faraday Trans.* **91** (1995) p. 937.
29. Branton P.J., Hall P.G., Sing K.S.W., Reichert H. and Schueth F., Unger K.K., Physisorption of argon, nitrogen and oxygen by MCM-41, a model mesoporous adsorbent, *J. Chem. Soc. Faraday Trans.* **90** (1994) pp. 2965-2967.
30. Schmidt, Stoecker M., Hansen E., Akporiaye D. and Ellestad O.H., MCM-41: a model system for adsorption studies on mesoporous materials, *Microporous Materials* **3** (1995) pp. 443 -448.
31. Llewellyn P.L., Grillet Y., Schueth F. and Reichert H., Unger K., Effect of pore size on adsorbate condensation and hysteresis within a potential model adsorbent: M41S, *Microporous Mater.* **3** (1994) p. 345.
32. Llewellyn P.L., Grillet Y., Ruquerol J., Martin C. and Coulomb J.P., Thermodynamic and structural properties of physisorbed phases within the model mesoporous adsorbent M41S (pore diameter 2.5 nm), *Surf. Sci.* **352 - 354** (1996) pp. 468.
33. Ravikovitch P. I., Domhnaill S.C.O., Neimark A.V. and Schueth F., Unger K.K., Capillary hysteresis in nanopores: Theoretical and experimental studies of nitrogen adsorption on MCM-41, *Langmuir* **11** (1995) pp. 4765 – 4772.
34. Zhu G.Y., Zhao X.S., Lu G.Q. (Max) and D.D.Do., Improved comparison plot method for pore structure characterization of MCM-41, *Langmuir* **12** (1996) pp. 6513-6517.
35. Maddox M.W., Olivier J.P. and Gubbins K.E., Characterization of MCM-41 using molecular simulation heterogeneity effects, *Langmuir* **13** (1997) pp. 1737-1745.
36. Kruk M., Jaroniec M. and Sayari A., Adsorption study of surface and structural properties of MCM-41 materials of different sizes, *J. Phys. Chem. B* **101** (1997) pp. 583-589.
37. Sonwane C.G., Bathia S.K. and Calos N., Experimental and theoretical investigation of adsorption hysteresis and criticality in MCM-41: Studies with O<sub>2</sub>, Ar and CO<sub>2</sub>, *Ind. Eng. Chem. Res.* **37** (1998) pp. 2271- 2283.
38. Lukens W.W. Jr., Schmidt-Winkel, Zhao D., Feng J. and Stucky G.D., Evaluating pore sizes in mesoporous materials: a simplified standard adsorption method and a

- simplified Broeckhoff-de Boer method, *Langmuir* **15** (1999) pp. 5403-5409.
39. Kruk M. and Jaroniec M., Characterization of the porous structure of SBA-15, *Chem. Mater.* **12** (2000) pp. 1961-1968.
40. Ravikovitch P.I. and Neimark A.V., Characterization of micro-and mesoporosity of SBA-15 materials from adsorption isotherms by the NLDFT method *J. Phys. Chem B* **105** (2001) pp. 6817 – 6823.
41. Romero A.A., Alba M.D., Zhou W. and Klinowski J., Synthesis and characterization of the mesoporous silicate molecular sieve MCM-48, *J. Phys. Chem B.* **101** (1997) pp. 5294-5300.
42. Kruk M., Jaroniec M., Ryoo R. and Kim J.M., Characterization of MCM-48 silicas with tailored pore sizes synthesized via a highly efficient procedure, *Chem Mater.* **11** (1999) pp. 2568-2572.
43. Thommes M., Koehn R., Froeba M., Systematic sorption studies on surface and pore size characteristics of different MCM-48 silica materials, *Studies in Surface Science and Catalysis* **128** (2000) pp. 259-269.
44. Thommes M., Koehn R. and Froeba M., Sorption and pore condensation behavior, of nitrogen, argon and krypton in mesoporous MCM-48 silica materials, *J. Phys. Chem B* **104** (2000) pp. 7932-7943.
45. Schumacher K., Ravikovitch P., Du Chesne A. and Neimark A.V., Unger K.K., Novel Characterization of MCM-48 materials, *Langmuir* **16** (2000) pp. 4648 – 4654.
46. Kruk M. and Jaroniec M., Characterization of MCM-48 silicas with tailored pore sizes synthesized via a highly efficient procedure, *Chem Mater.* **12** (2000) pp. 1414 – 1421.
47. Ravikovitch P.I. and Neimark A.V., Relations between structural parameters and adsorption characterization of templated nanoporous materials with cubic symmetry, *Langmuir* **16** (2000) pp. 2419 – 2423.
48. Thommes M., Koehn R. and Froeba M., Characterization of mesoporous solids: pore condensation and hysteresis phenomena in mesoporous molecular sieves. *Studies in Surface Science and Catalysis* **142** (2002) pp. 1695 -1702.
49. Kanda H., Myahara M., Yoshioko T. and Okazaki M., Verification of the condensation model for cylindrical nanopores. Analysis of the nitrogen isotherm for FSM-16, *Langmuir* **16** (2000) pp. 6622-6627.
50. Inohue S., Hanzwa Y. and Kaneko K., Prediction of hysteresis disappearance in the adsorption isotherm of N<sub>2</sub> on regular mesoporous silica, *Langmuir* **14** (1998) pp. 3079-3081.
51. Darmstadt H., Roy C., Kaliaguine S., Choi S.J. and Ryoo R., Surface Chemistry of mesoporous carbon molecular sieves, *Carbon* **40** (2002) pp. 2673 – 2683.
52. Gregg S.J. and Sing K.S.W., *Adsorption, Surface Area and Porosity* (Academic Press, London, 1982).
53. Lowell S. and Shields J.E., *Powder Surface Area and Porosity* (Chapman & Hall, London, 1991).
54. Rouquerol F., Rouquerol J. and Sing K. S.W., *Adsorption by Powders & Porous Solids* ( Academic Press, London, 1999).
55. Galarneau A., Desplandier D., Dutartre R. and Di Renzo F., Micelle-templated silicates as a test bed for methods of mesopore size evaluation, *Microporous Mesoporous Mater.* **27** (1999) pp. 297-308.
56. Rouquerol F., Rouquerol J., Peres C., Grillet Y. and Boudellal M., Calorimetric

- study of nitrogen and argon adsorption on porous silicas, In *Characterization of Porous Solids*, edited by Gregg S.J, Sing K.S.W, Stoeckli H.F. (The Society of Chemical Industry, Luton ,UK, 1979) pp. 107 – 116.
57. Jelinek L. and Kovats E.S., True surface area from nitrogen adsorption experiments, *Langmuir* **10** (1994) pp. 4225 – 4231.
  58. Pfeifer P., Avnir D. and Farin D., Scaling Behavior of Surface Irregularity in the molecular Domain: From Adsorption studies to fractal catalysts, *Journal of Statistical Physics* **36** (1984) pp. 699-717.
  59. Neimark A. V. and Unger K.K., Method of discrimination surface fractality, *Journal of Colloid and Interface Sci.* **158** (1993) pp. 412-419.
  60. Sonwane C.G., Bhatia S.K. and Calos N.J., Characterization of surface roughness of MCN-41 using methods of fractal analysis, *Langmuir* **15** (1999) pp. 4603-4612
  61. Barrett E. P., Joyner L. G., and Halenda P. P., The determination of pore volume and area distributions in porous substances. I Computations from Nitrogen Isotherms, *J. Amer. Chem. Soc.* **73** (1951) pp. 373-380.
  62. Broekhoff J.C.P., de Boer J.H., Studies on pore systems in catalysts. IX. Calculation of pore distributions from the adsorption branch of nitrogen sorption isotherm in the case of open cylindrical pores. A. Fundamental equations, *J. Catalysis* **9** (1967) pp. 8-14.
  63. Broekhoff J.C.P. and de Boer J.H., Studies on pore systems in catalysts XIII. Pore distributions from the desorption branch of a nitrogen sorption isotherm in the case of cylindrical pores, *J. Catalysis* **10** (1968) pp. 377 -380; XIV. Calculation of the cumulative distribution functions for slit-shaped pores from the desorption branch of a nitrogen isotherm, *J. Catalysis* **10** (1968) pp. 391-400.
  64. Broekhoff J.C.P., de Boer J.H., Calculation of pore distributions from the adsorption branch of nitrogen sorption isotherm in the case of open cylindrical pores. B. Applications *J. Catalysis* **9** (1967) pp. 15-27.
  65. Cole M. W. and Saam W. F., Exitation spectrum and thermodynamic properties of liquid films in cylindrical pores, *Phys.Rev.Lett.* **32** (1974) pp. 985-988.
  66. Evans R. J., Fluids adsorbed in narrow pores: phase equilibria and structure, *Phys. Condens Matter* **2** (1990) pp. 8989-9006.
  67. Votyakov E.V., Tovbin Y.U.K., MacElroy J.M.D. and Roche A., A theoretical study of the phase diagrams of simple fluids confined within narrow pores, *Langmuir* **15** (1999) pp. 5713 – 5721.
  68. Celstini F., Capillary condensation within nanopores of various geometries, *Physics Letters A* **228** (1997) pp. 84 -90.
  69. Gubbins K. E., Theory and simulation of adsorption in micropores, In *Physical Adsorption: Experiment, Theory and Application*, edited by J. Fraissard, (Kluwer, Dordrecht, 1997) pp. 65 -105.
  70. Gelb L.D., Gubbins K.E., Radhakrishnan R. and Sliwinska-Bartkowiak M., Phase separation in confined systems, *Rep. Prog. Phys.* **62** (1999) pp. 1573 -1659.
  71. Burgess C.G.V., Everett D.H. and Nuttall S., Adsorption hysteresis in porousmaterials, *Pure & Appl. Chem.* **61** (1989) pp. 1845-1853.
  72. De Keizer A., Michalski T. and Findenegg G.H., Fluids in pores: experimental and computer simulation studies of multilayer adsorption, pore condensation and critical-point shifts, *Pure & Appl. Chem.* **63** (1991) pp. 1495-1502.
  73. Thommes M. and Findenegg G.H., Pore condensation and critical-point shift of a fluid in controlled-pore glass, *Langmuir* **10** (1994) pp. 4270-4277.

74. Machin W. D., Temperature dependence of hysteresis and the pore size distribution of two mesoporous adsorbents, *Langmuir* **10** (1994) pp. 1235 – 1240.
75. Groß S. and Findenegg G.H., Pore condensation in novel highly ordered mesoporous silica, *Ber. Bunsenges. Phys. Chem.* **101** (1997) pp. 1726-1730.
76. <sup>a</sup>Morishige K. and Shikimi M., Capillary critical point of argon, nitrogen, oxygen, ethylene and carbon dioxide in MCM-41, *Langmuir* **13** (1997) pp. 3494-3498.  
<sup>b</sup>Morishige K. and Shikimi M., Adsorption hysteresis and pore critical temperature in a single cylindrical pore, *J. Chem Phys.* **108** (1998) pp. 7821-7824.
77. Sonwane C.G. and Bhatia S.K., Characterization of pore size distribution of mesoporous materials from adsorption isotherms, *J. Phys. Chem B* **104** (2000) pp. 9099-9110; Bhatia S.K., and Sonwane C.G., Capillary coexistence and criticality in mesopores: modification of the Kelvin theory, *Langmuir* **14** (1998) pp. 1521-1524.
78. Myahara M., Sakamoto M., Kandra H. and Higashitani K., Freezing point elevation in nanospace detected directly by atomic force spectroscopy, *Studies in Surface Science and Catalysis* **144** (2002) pp. 411 – 418.
79. Olivier J., Thermodynamic Properties of confined fluids I : Experimental measurement of krypton adsorbed by mesoporous silica from 80 K to 130 K, In *Proceedings of the Second Pacific Basin Conference on Adsorption Science and Technology*, edited by D.D. DO ( World Scientific, Singapore, 2000) pp. 472 - 476.
80. Fretwell H.M., Duffy J.A., Clarke A.P., Alam M.A. and Evans R., Phase Transitions of CO<sub>2</sub> confined in nanometer pores as revealed by positronium annihilation *J. Phys. : Condens Matter* **7** (1995) pp. L717-L717.
81. Coulomb J.P., Grillet Y., Lewellyn P.L., Martin C. and Andre G., Structural properties of krypton confined in MCM-41 ( $\phi = 40 \text{ \AA}$ ) In *Fundamentals of Adsorption*, edited by F. Meunier ( Elsevier, Paris, 1998) pp. 147 – 152.
82. Morishige K., Kawano K. and Hayashigi T., Adsorption isotherm and freezing of Kr in a single cylindrical pore, *J. Phys. Chem B* **104** (2000) pp. 10298-10303.
83. Huber P. and Knorr K., Adsorption-desorption isotherms and x-ray diffraction of Ar condensed into a porous glass matrix, *Phys. Rev. B* **60** (1999) pp. 12657 – 12665.
84. Dominguez H., Allen M.P. and Evans R., Monte Carlo Studies of the freezing and condensation transition of confined fluids, *Mol. Phys.* **96** (1998) pp. 209-229.
85. De Boer J. H., *The Structure and Properties of Porous Materials*, (Butterworth, London, 1958).
86. Everett D.H., Adsorption hysteresis, In *The Solid-Gas Interface Vol.2*, edited by E.A. Flood ( Marcel Decker, New York, 1967).
87. Ball P.C. and Evans R., Temperature dependence of gas adsorption on a mesoporous solid : capillary criticality and hysteresis, *Langmuir* **5** (1989) pp. 714-723.
88. Neimark A.V., Ravikovitch P.I. and Vishnyakov A., Adsorption Hysteresis in nanopores, *Phys. Rev. E* **62**, (2000) p. R1493.
89. Neimark A.V. and Ravikovitch P.I., Capillary condensation in MMS and pore structure characterization, *Microporous and Mesoporous Materials* **44-56** (2001) pp. 697-707.
90. Awschalom D.D., Warnock J. and Shafer M.W., Liquid-film instabilities in confined geometries, *Phys. Rev. Lett.* **57** (1996) pp. 1607 -1610.

91. Mason G., The effect of pore space connectivity on the hysteresis of capillary condensation in adsorption-desorption isotherms, *J. Colloid Interface Sci.* **88** (1982) pp. 36-46.
92. Wall G. C. and Brown R. J. C., The determination of pore size distributions from sorption isotherms and mercury penetration in interconnected pores: the application of percolation theory, *J. Colloid Interface Sci.* **82** (1981) p. 141.
93. Neimark A.V., Percolation theory of capillary hysteresis phenomena and characterization of porous solids, *Studies in Surf. Sci. & Catal.* **62** (1991) pp. 67-74.
94. Parlar M. and Yortsos Y.C., Percolation theory of vapor adsorption-desorption processes in porous materials, *J. Colloid Interface Sci.* **124** (1988) pp. 162 – 176.
95. Zhu H., Zhang L. and Seaton N. A., Sorption hysteresis as a probe of pore structure, *Langmuir* **9** (1993) pp. 2576 - 2582; Liu H., Seaton N.A., Determination of the connectivity of porous solids from nitrogen sorption measurements - III Solids containing large mesopores, *Chem. Eng. Sci.* **49** (1994) pp. 1869 - 1879.
96. Rojas F., Kornhauser I., Felipe C., Esparza J.M., Cordero S., Dominguez A., and Riccardo J.L., Capillary condensation in heterogeneous mesoporous networks consisting of variable connectivity and pore-size correlation, *Phys.Chem.Chem.Phys.* **4** (2002) pp. 2346-2355.
97. Page J.H., Liu L., Abeles B., Herbolzheimer E., Deckmann H.W. and Weitz D.A., Adsorption and desorption of a wetting fluid in vycor studied by acoustic and optical techniques, *Phys. Rev. E*, **52**, (1995) pp. 2763-2777.
98. Hoinkis E. and Roehl-Kuhn B., The spatial distribution of vapor-filled voids on condensation and drainage of nitrogen at ~ 78 K in a mesoporous silica glass. In *Fundamentals of Adsorption 7*, edited by Kaneko K., Kanoh H., Hanzawa Y., (IK International ltd, Chiba City, Japan ,2002) pp. 601 -607.
99. Sarkisov L. and Monson P.A., Modelling of adsorption and desorption in pores of simple geometry using molecular dynamics, *Langmuir* **17** (2001) pp. 7600 – 7604.
100. Gubbins K.E., Molecular simulation of confined nano-phases. In *FundamentalsOf Adsorption 7*, edited by Kaneko K., Kanoh H., Hanzawa Y., (IK International Ltd, Chiba City, Japan , 2002) pp. 17-20.
101. Page K.S. and Monson P.A., Monte Carlo calculations of phase diagrams for a fluid confined in a disordered porous material, *Phys. Rev. E*, **54** (1996) pp. 6557 - 6564.
102. Pellenq R.J.M., Rousseau B. and Levitz P.E., A grand canonical monte carlo study of argon adsorption/condensation in mesoporous silica glasses, *Phys. Chem.Chem. Phys.* **3** (2001) pp. 1207 – 1212.
103. Gelb L.D. and Gubbins K.E., Characterization of porous glasses: Simulation models, adsorption isotherms, and the BET analysis method, *Langmuir* **14** (1998) pp. 2097 – 2111.
104. Gelb L.D., Molecular simulation of capillary phenomena in controlled pore Glasses, in *Fundamentals of Adsorption 7*, edited by Kaneko K., Kanoh H. and Hanzawa Y., ( IK International ltd, Chiba City, Japan, 2002) pp. 333 – 340.
105. Kierlik E., Rosinberg M.L., Tarjus G., and Viot P., Equilibrium and out-of equilibrium (hysteretic) behavior of fluids in disordered porous materials: Theoretical predictions, *Phys. Chem.Chem. Phys* **3** (2001) pp. 1201-1206.
106. Woo H.J., Sarkisov L. and Monson P.A., Mean-field theory of fluid adsorption in a porous glass, *Langmuir* **17** (2001) pp. 7472-7475.

107. Burgess C.G.V. and Everett D.H., The lower closure point in adsorption hysteresis of the capillary condensation type, *J. Colloid and Interface Sci* **33** (1970) p. 611.
108. Sonwane C.G. and Bhatia S.K., Analysis of criticality and isotherm reversibility in regular mesoporous materials, *Langmuir* **15** (1999) pp. 5347-5354.
109. Ravikovitch P.I. and Neimark A.V., Experimental confirmation of different mechanisms of evaporation from ink-bottle type pores: equilibrium, pore blocking, and cavitation, *Langmuir* **18** (2002) pp. 9830 – 9837.
110. Schreiber A., Reinhardt S. and Findenegg G.H., The lower closure point of the adsorption hysteresis loop of fluids in mesoporous silica materials, *Studies in Surface Science and Catalysis* **144** (2002) p. 177.
111. Zhu H.Y., Ni L.A. and Lu G.Q. (Max), A pore size dependent equation of state for multilayer adsorption in cylindrical mesopores, *Langmuir* **15** (1999) pp. 3632-3641.
112. Sonwane C.G. and Bhatia S.K., Determination of pore size distributions of mesoporous materials from adsorption isotherms, in *Fundamentals of Adsorption* **7**, edited by Kaneko K., Kanoh H. and Hanzawa Y., (IK International Ltd, Chiba City, Japan, (2002) pp. 999 – 1006.
113. Groen J.C., Doorn M.C. and Peffer L.A.A., MCM-41 and the BDB corrected Kelvin equation for accurate mesopore size distributions from gas adsorption data, in *Adsorption Science and Technology*, edited by D.D. Do (World Scientific, Singapore, 2000) pp. 229-233.
114. Kruk M. and Jaroniec M., Application of large pore MCM-41 molecular sieves to improve pore size analysis using nitrogen adsorption measurements, *Langmuir* **13** (1997) pp. 6267 – 6273.
115. Jaroniec M., Kruk M. and Choma J., The 50<sup>th</sup> anniversary of the Barrett-Joyner-Halenda method for mesopore size analysis: critical appraisal and future Perspective, in *Fundamentals of Adsorption* **7**, edited by Kaneko K., Kanoh H. and Hanzawa Y., ( IK International Ltd, Chiba City, Japan, 2002) pp. 570 – 577.
116. Kruk M. and Jaroniec M., Accurate method for calculating mesopore size distributions from argon adsorption data at 87 K developed using model MCM-41 materials, *Chem. Mater.* **12** (2000) 222-230.
117. Kruk M. and Jaroniec M., Determination of mesopore size distributions from argon adsorption data at 77 K, *J. Phys. Chem B* **106** (2002) 4732 – 4739.
118. Kruk M., Antochshuk V., Jaroniec M. and Sayari A., New Approach to evaluate pore size distributions and surface areas for hydrophobic mesoporous solids *J. Phys. Chem B* **103** (1999) pp. 10670 – 10678.
119. Evans R., Marconi U. M. B., and Tarazona P., Fluids in narrow pores: adsorption, capillary condensation and critical points *J. Chem. Phys* **84** (1986) pp. 2376-2399; Evans R., Marconi U. M. B. and Tarazona P., Capillary Condensation and adsorption in cylindrical and slit-like pores, *Chem. Soc, Faraday Trans 2*, **82** (1986) pp. 1763-1787.
120. Seaton N.A., Walton J.R.B. and Quirke N., A new analysis method for the determination of the pore size distributions of porous carbons from nitrogen adsorption measurements, *Carbon* **27** (1989) p. 853.
121. Lastoskie C.M., Gubbins K. and Quirke N., Pore size distribution analysis of microporous carbons: a density functional theory approach, *J. Phys. Chem.* **97** (1993) p. 4786.
122. Olivier J.P., Conklin W.B. and v. Szombathley M., Determination of pore size

- distribution from density functional theory, in *Studies in Surface Science and Catalysis* **87** (1994) p. 81.
123. Neimark A.V., Method of indeterminate Lagrange multipliers in the non-local density functional theory 124, *Langmuir* **11** (1995) p. 4183.
  124. Neimark A.V., Ravikovitch P.I., Grün M., Schüth F. and Unger K.K., Pore size analysis of MCM-41 type of adsorbents by means of nitrogen and argon adsorption, *J. Colloids and Interface Sci.* **207** (1998) pp. 159 – 169.
  125. Ravikovitch P.I. and Neimark A.V., Characterization of nanoporous materials from adsorption and desorption, *Colloids and Surfaces A: Physicochemical and Engineering Aspects* **187-188** (2001) pp. 11 – 21.
  126. Di Renzo F., Galarneu A., Trens P., Taunichoux N. and Fajula F., Confinement at nanometer scale: why and how? *Studies in Surface Science and Catalysis* **142** (2002) pp. 1057-1066.
  127. Neimark A.V., Ravikovitch P.I., and Vishnyakov A., Bridging scales from molecular simulations to classical thermodynamics: density functional theory of capillary condensation in nanopores, *J. Phys.: Condens. Matter* **1** (2003) pp. 347 – 365.
  128. Findenegg G.H., Gross S. and Michalski T., Pore condensation in controlled-pore glass. An experimental test of the Saam-Cole theory, *Studies in Surface Science and Catalysis* **87** (1994) pp. 71 -80.
  129. Smarsly B., Goeltner C., Antonietti M., Ruland W. and Hoinkis E., SANS Investigation of nitrogen sorption in porous silica, *J. Phys. Chem. B* **105** ( 2001) pp. 831-840; Smarsly B., Thommes M. and Ravikovitch P., manuscript in preparation.